ADVANCES
IN
ELECTROMETALLURGY

No. 1 Volume 9 2011

ELECTROSLAG TECHNOLOGY

Improving the quality of large ingots

F.K. Biktagirov, V.A. Shapovalov, M.V. Efimov, A.A. Selyutin and V.G. Padalka

E.O. Paton Electric Welding Institute, Kiev; Energomashspetsstal', Kramatorsk

Analysis of modern methods of improvement of the quality of large forged ingots was made. It was noted that most of them are based on electroslag technologies. It is shown that the electroslag heating of the riser in combination with hot topping improves the structure of the head part, increasing the yield of efficient metal and improving the homogeneity of the ingot as a whole.

Many branches of industry require large steel forgings for the manufacture of important components and sections (the rotor of turbines and generators, elements of the casings of atomic and chemical reactors and heat exchangers, ship shafts, the rolls of rolling mills, etc). The quality of these forgings determines the reliability and longevity of the components produced from them.

The quality of the large forgings is determined by the quality of initial ingots which may weigh up to several hundreds of tonnes.

The production of the large ingots is associated with the very complicated problem of both organisation and ensuring the required level of the quality of metal. The latter is associated with the fact that the long holding time of the large mass of the multicomponent liquid metal is accompanied by the formation in the resultant ingot of different defects of the shrinkage and liquation origin. The ingot is produced with non-uniform chemical composition and the density in different

volumes, and the nonuniformity increases with increasing mass of the ingot.

The main defects of the steel ingots are shrinkage cavities and porosity; axial (V-shaped) and off-centre (Λ-shape) liquation; local clusters of gases and nonmetallic inclusions.

As indicated by the results of ultrasonic inspection of ingots weighing more than 100 t and produced by the Izhorsk Plant and Japan Steel Works [1] and also by the Energomashspetsstal company, the largest problem regarding this type of the defects is the axial zone of ingots in the upper half. In addition to the shrinkage cavities and cavities below the riser, there is also a general and local increase of the concentration of liquating impurities, non-metallic inclusions and gases.

In order to ensure the maximum possible physical density of the ingot, which controls the chemical uniformity of the ingot, in the process of formation of the ingot it is necessary to exclude the formation of transverse

constrictions and 'bridges' which inhibit the supply of liquid metal to the low-lying layers with shrinkage.

To fulfil these requirements, it is necessary to maintain a positive temperature gradient of the metal in the direction to the top part of the ingot. For this purpose, i.e. riser attachment with a heat-insulating side surface is placed on the mould, and the conicity of the ingot moulds also increases. The mass of the metal of the riser of the large ingots reaches 25% and more of the mass of the entire liquid metal poured into the mould (with the riser attachment). The chemical homogeneity and physical density of the ingot are also improved by the reduction of the content of undesirable impurities and elements which extensively liquate and causes the formation of a coarse crystalline structure.

Improvement of the structure of the top part of the large ingots is important from the viewpoint of not only increasing the quality of the ingot as a whole but also from the economic viewpoint (reduction of the consumption of liquid metal and increase of the yield of acceptable metal). The increase of the purity of the initial liquid metal, improvement of the design of the mould and the riser help in improving the structure of large ingots [2–4].

However, these measures do not always make it possible to reach the high level of integrity and homogeneity of the ingots, especially in the conditions of continuously increasing requirements on quality. Therefore, investigations are being carried out to examine the nature of formation of various defects and find methods of preventing their formation.

The application for this purpose of traditional methods (improved heat insulation of the side surface of the riser attachment, increase of the temperature of the metal surface by heat-insulating and exothermic mixtures, etc) doesn't make it possible, because of the large volumes of metal in the size of part and long solidification time, to influence sufficiently the course of solidification of the large ingots [5].

Various methods of additional hot topping

the riser are more efficient. Heating can be by gas, electric arc, induction or electroslag.

Electroslag technologies are used most frequently in practice as a result of a number of reasons, with the main reasons being the more uniform and controlled heating of the surface of the metal of the entire surface and the possibility of simultaneous refining of the metal with the slag.

The electroslag process in which the consumable metallic blank is gradually melted in the thickness of the molten slag has been used as the starting point for the development of the method of electroslag remelting (ESR) which is recommended as one of the most efficient methods of production of high quality metal products. ESR is also used for the production of large ingots from medium-alloy steels, in particular, the Cr–Ni–Mo system.

However, an increase of the mass and diameter of the ingot makes it more difficult to ensure directional solidification (this is the main prerequisite for the production of high quality blanks) in classic ESR. In addition, the production of the ingots by these methods is demanding on energy and requires considerable capital and actual investment, including for the production of consumable electrodes. ESR has been used as the basis for developing other cheaper technologies in which the solidified metal can be influenced [5]. They include (after practical testing and application, electroslag heating and feeding, electroslag casting (pouring) [6–8], BEST and TREST processes [10–13], the MXKW method and portional electroslag casting (PEC) [14–16].

The main aim of electroslag heating is to reduce the size of the shrinkage cavity and increase the yield of suitable metal. The experts at the E.O. Paton Electric Welding Institute developed this technology efficiently for a number of metallurgical and engineering plants already at the end of the 1950s and the beginning of 1960s.

In this method, a special watercooled or lined attachment is placed on the cast iron ingot moulds. After filling with liquid metal, the slag is melted in the attachment using a non-consumable electrodes and is held in the

superheated condition.

The composition of the slag is selected taking into account the requirements on the stable control of the electroslag process in the given temperature conditions. The formation of the ingot is accompanied by electroslag heating of the metal surface to ensure free feed of liquid metal to the solidifying parts and preventing the formation of the closed and deep shrinkage cavity [6, 8].

Electroslag heating improves the structure of the top part of the ingot and is used mostly for preventing the formation of shrinkage defects. It should be mentioned that electroslag heating ensures the refining of the metal volumes in the vicinity of the slag and the reduces the size of the zone of negative liquation in the bottom part of the ingot.

The same procedure is used for electroslag feeding of the riser part of the ingot, only in this case metallic consumable electrode, i.e., electrodes which melt in the slag, are used instead of non-consumable electrodes.

From the viewpoint of sealing the riser, feeding has both shortcomings and advantages in comparison with heating. The main advantage is that the metal required for compensating shrinkage is supplied by the consumable electrode so that the shrinkage cavity can be displaced and the head part with maximum density throughout the entire height is produced. In addition, the chemical composition of the electrode can be selected taking into account correction of the composition of metal in the top part of the ingot.

Shortcomings include the need to produce a consumable electrode, preparation and pouring the liquid metal in the starting period, more stringent requirements of the composition and properties of the slag (electrical conductivity, viscosity), the presence of but on current supply with the single-phase single-electrodes feed circuit, complicated regulation of the masts melting rate of each electrode in bifilar and three-phase circuits of current supply, more complicated equipment.

The selection of the technology of electroslag heating or electroslag feeding is determined depending on the specific conditions and possibilities of the plant. It should be taken into account that in electroslag heating it is possible to compensate shrinkage as a result of supplying into the slag pool of the metal in the form of non-compacted fragmented material (shavings, cutting pieces, dust, etc) or an electrode without current which melts in the slag.

Experiments carried out with the electroslag heating of the riser part of the ingot to influence more efficiently the conditions of transfer of a metal from the liquid to solid state were used as the basis for the development of the method of electroslag casting (ESC) which combines the advantages of electroslag heating, refining of the metal with the slag and casting under a slag [9]. The method is based on the following procedure.

Initially, the slag pool is produced and heated to the required temperature in the watercooled mould using nonconsumable electrodes. Subsequently, the liquid metal is poured into the mould through the slag and the liquid metal subsequently solidifies in electroslag heating in the conditions of displacement of the shrinkage cavity with a gradual reduction of the power supplied to the slag pool. After completing heating and solidification of the slag and the metal, the resultant ingot is extracted from the mould.

In this technology, various procedures can be used for the method. For example, the entire described process can be realised in a watercooled solidification mould placed on a flat watercooled baseplate, or on a watercooled baseplate, including the entire volume of the slag melt, there is a conventional cast iron mould and some riser attachment is placed on the top of the mould. In the latter case, the current conducting electrodes and gradually lifted upwards as the mould is filled.

The slag can be noted from the initial solid components directly in the solidification mould or it can be melted in a separate flux-melting furnace and poured into the solidification mould prior to casting the metal. The electrical circuit of the electroslag process can be single- or three-phased. Various methods of connecting the electrodes to

the power source can be used in both cases.

At the end of the 70s, information was published on application of the processes BEST and TREST for improving the quality of large ingots [10–13]. These methods represent a variety of the investigated method of electroslag feeding. In the first case, a riser watercooled attachments is placed on the mould, whereas a lined attachment displaced on the molten the second case.

According to the published data, the technology and production by these methods of forging and sheet ingots weighing up to 55 t has beenmastered and the quality of the ingots, especially of the upper part, is considerably higher in comparison with the ingots produced by conventional technology. Work is being carried out to increase the weight and widen the range of ingots produced by these two processes, to investigate the quality of these ingots and production of forging from them, including in comparison with the identical components produced from ESR ingots [14].

Another direction of production of large ingots is based on various methods of enlarging using the electroslag process (electroslag welding and surfacing, MXKW and ESC processes).

Electroslag welding is carried out on completed forgings which are welded together by the ends. This method, including the method using strip electrodes, was developed at the E.O. Paton Electric Welding Institute, Kiev, and has been used successfully in the manufacture of rotors of turbogenerators [15]. Recently, special interest has been paid to this method of electroslag welding as a possible method of producing super large blanks from several smaller ingots.

In the group of various variants of electroslag surfacing and enlarging for production of ingots with a large cross-section, the highest promise is offered by the method of circumferential electroslag surfacing with liquid filler metal (ESS LM) in which the metal is 'built up' on the blank in layers around the diameter [16, 17].

As a result of the comparatively small size of these layers and the volume of the metal pool, it is possible to produce ingots that are uniform in height and diameter. This technology has been tested most extensively in the production of ingots from complexly alloyed steels and alloys susceptible to liquation.

The MXKW is based on the following procedure [18]. The core is involved along the entire height of the ingot produced by conventional technology in a forging press, i.e., the main defective zone is involved. The resultant cavity is then melted up by electroslag melting with a consumable electrode. In addition to the complicated procedure and high cost, this technology is associated with problems with ensuring uniform and defect-free melting of the deposited metal with the body of the ingot and compensation of the unavoidable thermal stresses.

A unique method of enlargement is portional electroslag casting (PEC) in which the metal is supplied into the solidification mould in several portions [19, 20]. Initially, the first portion is poured through the liquid slag and this portion fills only part of the volume of the solidification mould. This is followed by electroslag heating of the metal surface in the conditions ensuring the liquid state of the top part of the portion. The poured-in metal gradually solidifies from bottom to top.

After some time when a small amount of liquid metal remains under the slag, the second portion is poured into the solidification mould and this portion is also held under electroslag heating and solidifies in the axial direction.

Similar pouring of the metal in small portions is repeated until the entire mould is filled. In the final stage of the formation of the ingot in portional electroslag casting, the power supplied to the slag pool is slowly reduced in order to displace the shrinkage cavity.

Equipment EShO-200I1, which started service at the Energomashspetsstal' company, this method was used to produce ingots weighing up to 75 t (diameter 1600 mm) and 200 t (diameter 2500 mm). On the whole, the technology of portional electroslag cast-

ing is quite efficient, as shown by investigations of the quality of the ingots [30]. As regards the cost of equipment, the equipment for portional electroslag casting is cheaper than similar types of the become and for electroslag remelting. However, the main advantage of equipment is the absence of consumable electrodes whose price represent a large fraction in the total production costs of the ESR ingots.

Thus, the quality of large steel ingots can be increased using these processes. They have been subjected to industrial and pilot plant verification and are of applied importance for companies specialising in the production of large blanks.

The leading Ukrainian company in this area is Energomashspetsstal', Kramatosk. In addition to relatively small ingots (3–90 t), the company produces products for important applications from ingots with the weight of 100-250 t. In 2010, the Energomashspetsstal' produced by casting for the first time in Ukraine three ingots weighing 355 t. The metal for these ingots was melted in electric arc furnaces followed by treatment in the ladle-furnace equipment, vacuum treatment in the ladle with blowing of argon and pouring into moulds, placed in vacuum chambers.

Taking into account the problems in production of large ingots, the company is investigating the possibility of improving the quality of these products by using one of the previously mentioned methods.

In future, the company is planning to start casting ingots weighing 420-450 t at the Energomashspetsstal' plant. In the production of these ingots, it is important to increase the yield of suitable metal because the reduction of the weight of the riser by 10% is equivalent to casting an ingot weighing approximately 500 t. The equipment installed in the company can be used for forging components from ingots of this weight and also for machining.

At the present time, the highest quality of the ingots is obtained in ESR, by the construction of super large equipment for ESR is an expensive project which maybe justified only if the equipment is fully loaded over

a long period of time. Nevertheless, many foreign companies are developing yourself furnaces for producing ingots weighing up to 450 t [21].

To a certain extent, this also relates to the technology of electroslag surfacing and portional electroslag casting, although the expenditure for realisation of these projects is slightly lower. Therefore, the metallurgical companies, specialising in the production of large ingots, can direct the effort to the development and introduction of processes combining the advanced technologies of melting and preparation of high-quality liquid steel with the technologies which improve the conditions of formation of the ingots, cast into the moulds. This may include various variants of electroslag casting, electroslag heating and hot topping.

In particular, the ingots weighing up to 50 t and more can be produced efficiently by electroslag heating of the riser part using non-consumable electrodes. A similar technology has been applied in heating the riser of large (up to 50 t) cast iron castings which not only reduce the weight of the riser but also improve the quality of cast rolls [22].
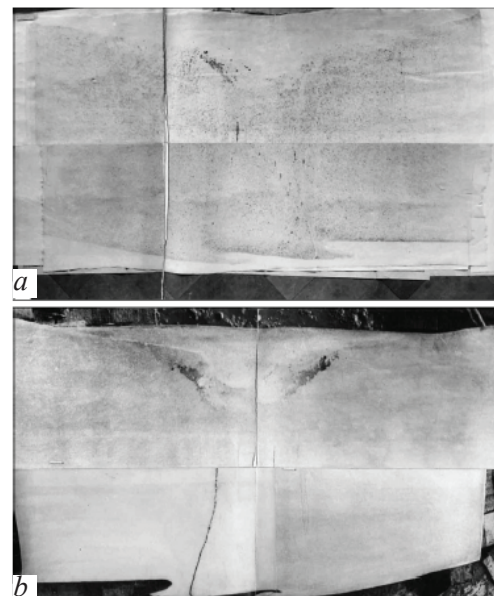
The literature contains reports (in most

Figure 1. Grey imprint (a) and macrostructure (b) of the axial templated of the top part of a 70 5t ingot produced by electroslag ???.

cases without any detail) on the application in Japan of the process of ESHT-J (electroslag hot topping Japan) in the production of steel ingots [23]. The method is based on electroslag heating of the metal in a lined riser attachment using three graphitised electrodes. It appears that this method is most efficient when used for large diameter ingots.

The large number of data, including the results obtained in direct investigations of the macrostructure, confirm that the influence on the solidification of metal in heating and feeding the riser not only saves metal by reducing the size of the riser in comparison with the ingots produced by conventional technology but also increases the density in the axial zone and reduces the general and local chemical heterogeneity.

Figure 1 shows the sulphur imprint and macrostructure of a longitudinal axial template of the top part of a 75 t ingot produced by electroslag casting from 10GN2MFA steel, produced in EShO-200I1 equipment. In contrast to the ingots produced by conventional technology, the large clusters of sulphur and sulphide inclusions are not found in this ingot. The existing 'whiskers' of off-axial heterogeneity are small in number and are very short. No axial porosity and V-shaped liquation was detected. The shrinkage cavity (open and shallow) at the axis of the ingot spreads to a depth of only 200–300 mm indicating the efficient selection of the conditions of electroslag heating and efficiency of this method. The positive effect was exerted by electroslag heating also on the structure of the bottom part of the ingot where the distinctive zone of negative liquation with reduced density of the metal did not form at all.

Conclusions

1. The electroslag heating of the top part of the ingot, including in combination with feeding, is a promising direction of improving the quality of large steel ingots.
2. In comparison with conventional casting, the structure of the upper and bottom part of the ingot is improved and the yield of suitable metal is greatly increased.

3. This method of improving the quality of ingots is efficient in the production of large steel castings, and electroslag heating of the risers of this casting guarantees the absence of shrinkage defects and greatly reduces the volume of the riser [24].

References

1. Afanas'ev S.Yu., et al., Elektrometallurgiya, 2006, No. 7, 37–39.
2. Dub V.S., et al., ibid, 1999, No. 5, 22–29.
3. Zhul'ev S.I., et al., Stal', 2005, No. 11, 41–44.
4. Tashiro K., et al., Transactions ISIJ, 1983, volume 23, 312–321.
5. Mitchell A., Sovremennaya Elektrometallurgiya, 2005, No. 2, 3–8.
6. Tyagun-Belous G.S. and Dudko D.A., Avt. Svarka, 1958, No. 10, 36–43.
7. Bakumenko S.P., et al., Reducing the waste in production of steel ingots, Metallurgiya, Moscow, 1967.
8. Marchenko I.K., Improving the quality of metal by electroslag heating the top part of the ingot, in: Advanced methods of producing steel ingots, Institute of Casting Problems, Kiev, 1980, 107–109.
9. Bastrakov N.F., et al., Electroslag casting of steel, Metallurgiya, Moscow, 1978.
10. Makhner P., et al., In: Electroslag remelting, No. 5, Naukova Dumka, Kiev, 1979, 259–266.
11. Makhner P., In: Electroslag remelting, No. 6, Naukova Dumka, Kiev, 1983, 306–316.
12. Bazevi S., et al., In: Electroslag remelting, No. 9, Naukova Dumka, Kiev, 1987, 317–321.
13. Maier V., et al., In: Electroslag remelting, No. 9, Naukova Dumka, Kiev, 1987, 159–153.
14. Kern T.U., et al., 17th Int. Forgemasters Meeting, Santander, Spain, 2008, 316–310.
15. Paton B.E., et al., in: Electroslag remelting, No. 1, Naukova Dumka, Kiev,, 1973, 234–243.
16. Paton B.E., et al., Sovremennaya Elektrometallurgiya, 2007, No. 1, 3–7.
17. Medovar L.B., et al., Sovremennaya Elektrometallurgiya, 2010, No. 3, 5–10.
18. Austel' W., et al., In: Electroslag remelting, No. 6. Naukova Dumka, Kiev, 1983, 301–305.
19. Paton B.E., et al., Spets. Elektrometall., 1973, No. 19, 24–29.
20. Latash Yu.V., et al., In: Electroslag remelting, No. 9, Naukova Dumka, Kiev, 1987, 78–84.
21. Medovar L.B., et al., Elektrometallurgiya, 2010, No. 11, 12–18.
22. Khrichikov V.E., et al., In: Saving metal as a result of widening the range and improving the quality of metal products, Proceedings of the National seminar, Moscow September, 1979.
23. Knyupel' G. and Makhner P., In: Electroslag remelting, No. 7, Naukova Dumka, Kiev, 1983, 60–61.
24. Nagaevskii V.I., et al., Spets. Elektrometllurgiya, 1984, No. 57, 38–40.

Some problems in the production of materials for power engineering

A.I. Balitskii and L.B.Medovar

G.V. Karpenko Physical-Mechanical Institute, Academy of sciences of Ukraine, Kiev;
E.O. Paton Electric Welding Institute, Kiev

Some problems of the technology of production of modern steels and alloys for power engineering are considered. Data are given for modern steels and alloys for application in heat turbines with 650–700°C operating temperatures. The technology of manufacture of band rings of high-nitrogen steels was analyzed. The role of electroslag remelting is shown. The challenging directions of works on improvement of materials and technologies of power machine building are described.

The energy safety of the country depends on many factors, in particular, on the state of energy-generating stations. Regardless of the high rate of development of nuclear power engineering, a large part of electrical energy in Ukraine is still produced and will be produced in thermal power stations.

At the same time, the condition of equipment in these stations requires careful consideration. The service life of several elements of the structures, working in gaseous hydrogen and (pressure vessels, the bodies of electrolysers, hydrogen drying systems, hydrogen transmission lines, rotors cooled by hydrogen and reinforcement bands) has already exceeded 50 years [1, 2].

Ageing and extensive wear of power equipment requires replacement and modernisation. At the same time, regardless of the existence of companies which can produce advanced energy equipment (Turboatomin Khar'kov, Zarya in Nikolaev), Ukraine does not possess equipment and technologies for producing appropriate advanced structural metallic materials [3–8]. The Ukrainian companies can produce only energy units of morally old-fashioned constructions or purchase advanced materials abroad (for example, for gas turbines in power engineering). In both cases, this does not satisfy the requirements for the energy safety of the country.

The existing situation is determined by the fact that the increase of efficiency (and ecological efficiency of power systems) is directly linked with the technological parameters of power units. As the working temperature and pressure in the turbine increase, the efficiency of the turbine increases (with other conditions being equal) and the amount of harmful substances emitted into the surrounding atmosphere decreases.

The lagging of Ukrainian power engineering in this aspect is well-known. For example, the level of working temperatures in the advanced steam turbines reaches 650°C, whereas Ukrainian power engineering systems work at 540–550°C, like 100 years ago. In addition, work is being carried out throughout the world to increase the working temperature above 700°C.

However, the increase of the parameters of the working temperature and pressure is not possible without application of new materials, and the development of these materials requires solution of a number of materials science, technological and organisation-technical problems, using materials of different types. In this article, it is attempted to analyse these problems and indicate the methods of solving them. There are two main types of turbines: steam and gas. They differ in the design features and technological parameters.

The gas turbines operate at considerably higher temperatures and, therefore, they are produced using complexly alloyed and more expensive alloys. At the present time, the temperature of the gases in the new class of gas power turbines, are referred to as the class F and H, reaches 1260 and 1427°C, respectively, whereas the working temperature of the advanced steam turbines usually does not exceed 650°C. Therefore, the rotors of the gas turbines are produced from nickel-based superalloys, and the rotors of the steam or steam-gas turbines are produced from alloyed or high-alloyed steels. (With transition to the working temperature of 700°C and higher, it

is also planned to use superalloys for steam turbines [5]).

Another problem is the absence of production in Ukraine of hydrogen-cooled rotors and reinforcement bands of turbo-generators in a wide range of powers, although in 1980–1990, there was experience with appropriate co-operation [9, 10]. Consequently, the rotating structures of the turbo-aggregates rapidly age, there are frequent hydrogen accidents, and Ukraine imports old-fashioned structures.

The development of power engineering requires constant improvement of metallic materials. To improve the working parameters of the energy units, it is necessary to use more complicated metallic materials. At the same time, the metallurgical quality of the blanks of the required size can be ensured using the melting and control of solidification (crystallisation) of these materials in the manufacture of large forging ingots.

In production of components from high-purity materials with a homogeneous structure for improvement of the efficiency of power engineering, it is important to use the most advanced technologies, such as vacuum melting of metals, vacuum-carbon deoxidation, vacuum-arc and electroslag remelting.
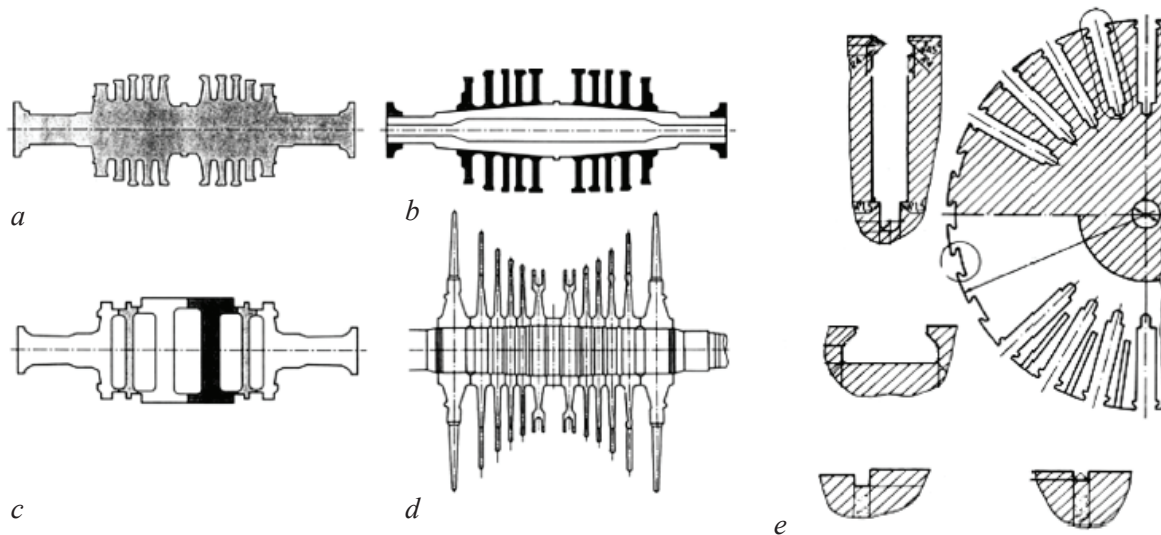

Fig. 1. Types of turbine rotor disks: a) all-forged; b, d) assembled (with attached disks); c) welded (consisting of individual disks – design of ABB Power Generation, Switzerland) [1, 10]: e) the barrel of the rotor of a turbo-generator with indication of the grooves for the wedges [2].

Electroslag remelting can be used not only for improving the quality of forging ingots but also for producing composite rotors, because in addition to the all-forged single-block rotors, the composite rotors are used on an increase in scale, especially for steam turbines (Fig. 1).

These rotors can be produced from different steels, satisfying the specific conditions of service of each section of the rotor. They are often produced by welding. However, welding of dissimilar steels in these sections is associated with considerable difficulties. Electroslag technology eliminates this problem and can be used to produce composite rotors with the improved (composite) structure.

Material science and the development of technological processes on the academic level correspond to foreign achievements in this area and are sometimes even more extensive, in contrast to industrial achievements. After the 1990s, no special advances have been made in the area of materials science for power engineering in Ukraine.

In the period 1950–1980, the steam turbines for thermal power stations, working with coal, were constructed mostly for the steam temperature of up to 550°C. The main material used for the production of high and medium pressure section was the Cr–Mo–V steel with 1% chromium (type 25KhN3MFA). The development of technology in the production of power units for steam turbines in Ukraine has remained on the same level since.

It has been noted that the parameters of the steam power units in the industrial developed countries have been greatly increased. Correspondingly, new materials have been developed and introduced into the industry. The effort of United Europe in the optimisation of the composition of steels and improvement of melting technology for transition to the temperatures of 550–600°C or higher has been efficiently utilised.

In Western Europe, these studies continued within the framework of general European special projects (COST (Cooperation in science and technology). For example, the main aim of the project COST 501 was the de-velopment of steels for service of rotors of steam turbines at temperatures of up to 600°C.

This project included the development of 9–12% chromium steels for large castings and forgings. Several grades of these steels have been developed with different hardening mechanisms and 22 rotors of steam turbines were produced from these steels in the 1990s for operation with the temperature of 600–625°C and pressure of up to 30 MPa with the maximum diameter of 1290 mm and weight of up to 45 t. These turbines are used in 14 thermal power stations with the power of up to 950 MW.

These studies were continued in the project COST 522 [11] to high-chromium martensitic steels for service at temperatures of 630–650°C. The basic material were steels of class of E with complex alloying with nitrogen, boron, cobalt and vanadium.

The COST 505 project was originated to produce a composite rotor EPRI-Europe with the diameters of the high-pressure section of 1250 mm and low pressure section of 1750 mm. 25 rotors of this type were produced within six years (from 1988 to 1994). Recently, work has continued in improving the technologies of production of the European rotor, and up to the 2000, the company Saarschmiede produced already 89 single-unit blanks for the rotors with the total weight of 2960 t.

The materials for service at temperatures higher than 600–650°C include austenitic steels and nickel-based alloys with inter-metallic hardening. Typical representatives of these materials are steel A-286, and also superalloys Inconel 706 and Inconel 718 used mainly for the manufacture of discs of aviation and energy gas turbines.

The common problems in the production of forgings for the rotors of the turbines produced from these materials are the problems associated with ensuring the stability of the composition and homogeneity of the structure of the metal.

The maximum diameter of the defect-free ingots for these alloys at the current industrial level of metallurgical technology

is usually not greater than 500–600 mm. In the Ukraine, there is almost no experience with the production of the superalloys and, according to expect evaluation, the level of metallurgical technology is not sufficiently high to melt ingots from these materials with the diameter greater than 400 mm.

At the same time, experts at the Academy of Sciences of Ukraine developed recently the advanced technologies of electroslag remelting of the superalloys which should help to overcome these obstacles. At the same time, without completing the appropriate innovation projects in the area of materials science it is not possible to produce advanced energy systems in Ukraine.

The usual evolution development of technology in this problem is interfered with by the paradoxic situation existing in Ukraine in which both the developers, producers and suppliers of the materials for power engineering are interested in their production but cannot change anything in this situation. The engineers often reject orders for the production of advanced energy units if there are no appropriate materials, and the metallurgists are not prepared to make any investment without having orders for such materials. Consequently, regardless of the current scientific potential and appropriate developments in the area of materials and technologies for engineering, Ukraine is stagnating in the development of this branch.

The existing situation can be solved by the development of a complex Ukrainian (on the basis of general European projects) energy program including the development and application by industry of the advanced materials for power engineering with participation of scientific organisations (IPM, IMF, IES, FMI NANU) and industrial companies (such as energomashspetsstal', Dneprospetsstal', NKMZ, Turboatom, Zarya-Mashproekt).

Some more detailed technical aspects of this program will be discussed later. For this purpose, we consider the individual stages of the technology of producing various important elements of advanced power systems, such as rotors and banding rings.

The rotors of steam and gas turbines were discussed extensively in the last World Meeting of Forgemasters in 2008 [12]. It should be mentioned that Ukrainian plants are now capable of producing casting ingots and forge components of rotors of steels with a higher chromium content. These companies include mostly NKMZ and Energomashspetsstal'. However, for transition to 12% chromium steel, it is necessary to have an electroslag remelting furnace with the capacity not smaller than 100 t. It should also be mentioned that in the period 2010–2011, no less than eight electroslag furnaces for melting ingots weighing from 100 to 450 t will start operation in the world [13].

The critical element of the energy system
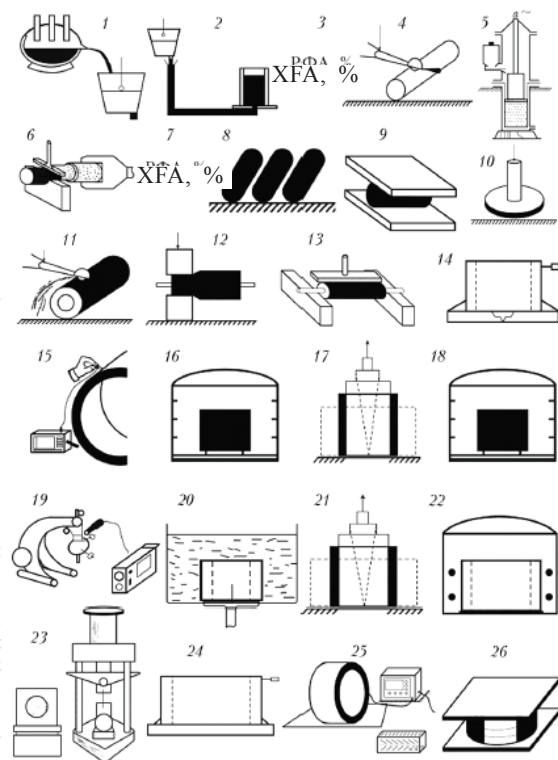
Fig. 2. Diagram of production of a banding ring, including the following operations: 1) melting; 2) casting of metal; 3) X fluorescent analysis (XFA); 4) turning; 5) electroslag remelting under pressure; 6) primary forging; 7) XFA; 8) cutting; 9) upsetting; 10) drilling; 11) abrasion; 12) slow forging; 13) expansion; 14) rough machining; 15) ultrasound flaw inspection; 16) heat treatment to the solid solution (HTSS); 17) quenching; 18) cold stretching (CS); 19) HTSS; 20) inspection of the structure; 21) CS; 22) removal of residual stresses; 23) device for examining the mechanical properties; 24) finishing machining; 25) nondestructive inspection; 26) packing.

is the banding ring. The technology of production of these components (Fig. 2) from high-nitrogen non-magnetic steels [14, 15–18], with the experience with manufacture of these components based on domestic metallurgical companies [9, 10] is based mostly on electroslag remelting.

After forging, the ring is heat-treated at $T = 1013–1070°C$ and quenched in water. Since the austenitic steels after hot pressure working or austenitising heat treatment are characterised by relatively low strength, the blanks of the rings are stretched in the cold condition (strain-hardened).

The majority of the rings are stretched hydraulically or mechanically and also by explosion. These operations with the result in high strength and the required dimensions but they should not reduce the level of plasticity and toughness below the permissible safe values.

The method of hydraulic stretching guarantees the relative uniformity of the mechanical properties around the perimeter of the ring, and the hardening in the internal surface and the residual compressive stresses, formed here, increase the load carrying capacity of bearing.

An additional advantage of this method is that the direction of the effect of the main working stresses (as regards the level) in the banding ring coincides with the direction of tensile loading. In the final stage of reduction, the rings are subjected to stabilising heat treatment at 350°C [19–26].

Electroslag remelting of high-nitrogen steels in the development of unique equipment for electroslag remelting have been discussed in a large number of studies [7–10]. The high-strength steels with the nitrogen content of approximately 1% are melted both in the conventional conditions (nitrogen is introduced together with the manganese and chromium master alloys) and in the furnaces with a higher nitrogen content.

The steels produced using special casting methods with the 'counter pressure' of nitrogen at a high (up to 1.4%) nitrogen content and without subsequent cold elastic treatment have the unique strength properties

for the quenched austenitic materials (yield strength may reach 1000 MPa) [2]. However, these technologies are not used on a large scale and the nitrogen content is traditionally restricted at 0.5%. In addition to electroslag remelting in the shielding atmosphere, the method of arc-slag remelting (ASR) can also be used [6, 7].

The results of industrial verification of arc slag remelting show that this method can be used to produce ingots of different cross-sections, with the satisfactory external surface and with the specific electrical energy consumption almost 1.5 times lower. The presence of the powerful electrical arcs in the melting zone of the metal in arc slag remelting in the nitrogen atmosphere creates suitable conditions for alloy in the steel with nitrogen. In arc slag remelting in nitrogen at higher pressure it is possible to alloy the steels with nitrogen directly from the gas phase up to superequilibrium nitrogen concentration. However, at present, the main process of producing the metal of the rings is the standard electroslag remelting at the atmospheric pressure, producing the steels of the type X18-G18 (18 Mn–18Cr) with the almost equilibrium nitrogen content.

The large number of the experiments, including the experiments in the production conditions, have been used as the starting point for the development of the technology of production of components for non-magnetic banding rings for turbo-generators from high-nitrogen steel 12Kh18AG18Sh for banding components, including for the turbo-generators with the power of 800 to 1200–1500 MW [8–10].

As regards the level of the corrosion and mechanical properties, the 12Kh18AG18Sh steel, produced in Ukraine by electroslag remelting, is similar to the Japanese 18Mn–18Cr and German P900 analogues with the extremely high values of the product of yield strength by fracture toughness K_{IC} $4.4 \cdot 10^5$ MPa^2 $\sqrt{m}$ [1].

The aim of this review is to attract attention to the problem described in the introduction. It is fully evident that without the advanced

materials there is no advanced energy power engineering. Without this information, it is not possible to discuss the energy safety of the country.

References

1. Balitskii O.I., Advanced materials for turbogenerators, L'viv, 1999.
2. Panasyuk V.D., Fracture mechanics and strength of materials, Akademperiodika, Kiev, 2005.
3. Paton B.E., et al., Sov. Elektrometallurgiya, 2004, No. 1, 3-9/
4. Medovar B.I., Arc slag remelting of steel and alloys, Cambridge Int. Sci. Publishing, Cambridge, 1996.
5. Large 718 forgings for land based turbines / R. C. Schwant, S. V. Thamboo, A. F. Anderson et al // Superalloys 718, 625, 706 and various derivatives: Proc. Intern. Symp. on Superalloys 718, 625, 706 and various derivatives. TMS (USA, Florida, June 15—18, 1997). – Florida, 1997. – P. 141—152.
6. Mitchell A., Sov. Elektrometallurgiya, 2005, No. 2, 3-8.
7. Paton B.E., et al., ibid, 2004 No. 3, 7-10.
8. Paton B.E., et al., ibid, 2007, No. 3, 3-7.
9. Balitskii A.I., Proc. 4th Int. Conf. Koroziya 98, L'viv, 1998, 151-154.
10. Voinov V.V., et al., in: High nitrogen steels, Proc. Conf., Kiev 1990, 411-412.
11. Vanstone R. W. Alloy design and microstructural control for improved 9...12% Cr power plant steels, Annex A, COST 522, Steam Power Plant, Final Report, 1998—2003. – P. 41—47.
12. Gianfrancesco A. Di. High Temperature Properties and Creep Behaviour of a CrMoCoB (FB2) Steel Trial Rotor // Proc. of the 17 th Intern. Forgemasters Meeting (Santander, Spain, Nov. 3—7, 2008). – Santander, 2008. – P. 36—40.
13. New Plant Concept for the Production of Large Sized Ingots / H. Holzgruber, B. Ofner, M. Ramprecht et al. // Proc. of the LMPC. – 2009. – P. 273—281.
14. Kutkin G.G., et al., High nitrogen steels, Proc. Conf., Kiev 1990, 8.
15. Pat. 4493733 USA, Int.Cl. 3 C22C38/58. Corrosion-Resistant Non-Magnetic Steel Retaining Ring for a generator / M. Yamamoto, T. Yebisuya T., M. Kamai, K. Tajima. – Publ. 15.01.85.
16. Balitskii A.I., et al., Author's Cert. 1488352, USSR MKI² C22C, 38/38, 23.06.89.
17. Balitskii A.I., et al., Author's Cert. 1668466, USSR MKI² C22, C 38/60, 07.08.91.
18. Balitskii A.I., et al., Author's Cert. 1488356, USSR MKI² C22, C38/38, 23.06.89.
19. Sorokin V.G., et al., Handbook of steels and alloys, Mashinostroenie, Moscow, 1989.
20. Stein G., Menzel J., Kirschner W. Manufacturing and operation of retaining rings made out of stress corrosion resistant steels // MaTeh' 1996: Proc. 1st Intern. conf. «Development, Testing and Application of Materials» (Opatija, Croatia, 2—5 Oct., 1996). – Opatija, 1996. – P. 203—208.
21. Stein G., Menzel I., Chowdhury A. Industrial manufacture of massive nitrogen-alloyed steels in a pressure ESR furnace // Steel times. – 1989. – 217, № 3. – P. 1461—150.
22. Stein G., Feichtinger H. Industrial usage of high nitrogen steels // Nitrogen Steels: Proc. conf. (Gliwice-Wisla, Poland, 24—26 Apr., 1996). – Gliwice-Wisla, 1996. – P. 5—16.
23. Menzel J., Kischner W., Stein G. High nitrogen containing Ni-free austenitic steels for medical applications // Ibid. – P. 139—148.
24. Lueg J., Kischner W., Stein G. CRONIDUR-alloys: Microstructure, properties and applications of HNS-martensitic steels // Ibid. – P. 189—196.
25. Production of non-magnetic rings from 18Cr—18Mn—0,5N2 steel under state steel industry conditions / B. Hoderny, J. Wiedermann, J. Bik, W. Pilecki // Ibid. – P. 197—204.
26. VSG Energie- und Schmiedetechnik Gmbh developed a new generation of steels. – Essen: VSG Energie- und Schmiedetechnik Gmbh, 1998. – 12 p.
27. Retaining Rings: Product Literature / Krupp Metal und Schmiedewerke. – Essen, 1990. – 54 p.
28. Balitskii A.I., et al., Avt. Svarka, 2003, No. 2, 28-31.
29. Balitskii A.I., et al., Sov. Elektrometallurgiya, 2004, No. 1, 55.
30. Balitskii A. I. Today and future welding // Physicochemical mechanics of materials. – 2003. – 39, № 6. – P. 118—120.
31. Balitskii A.I., et al., Sov. Elektrometallurgiya, 2004, No. 4, 56.
16. Balitskii A. I. Corrosion resistance of high nitrogen Cr—Mn steels and welding joining // Steel Grips. – 2004. – № 2. –P. 585—589.
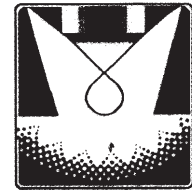
ELECTRON BEAM PROCESSES

Mathematical modelling of the process of dissolution of oxɣge n-containing refractory inclusions in a titanium melt

S.V. Akhonin, M.P. Kruglenko and V.I. Kostenko

E.O. Paton Electric Welding Institute, Kiev; Strategiya BM Company, Kiev

The mathematical model of the processes of dissolution of oxygen-containing titanium inclusions in the melt of titanium alloys is constructed and used to calculate the dependence of the rate of dissolution of the particle on the melt temperature. The dynamics of distribution of oxygen in the particles of α-titanium during dissolution is determined. The duration of complete dissolution of the oxygen-containing inclusions of titanium with different chemical composition and initial size is determined.

Introduction

One of the critical defects in titanium semi-finished products are the refractive inclusions in the form of particles of α-titanium with a higher content of the interstitial impurities stabilising this phase (nitrogen, oxygen and carbon), and also the chemical compounds of these elements with titanium (nitrides, oxides and carbides). In the literature, these inclusions are referred to as low-density inclusions (LDI) [1]. The hardness of these particles is considerably higher than that of the titanium matrix. Therefore, they act as stress concentrators and the sources of nucleation of fatigue cracks [1], resulting in the failure of important machine parts and, consequently, in malfunctions.

In most cases, the LDI inclusions form in the process of production of titanium sponge and consists to 95% of solid particles of α-titanium [1, 2]. These inclusions can be removed in the process of production of titanium ingots using the technologies of remelting in a cold hearth by gravitational precipitation [2–4] or dissolution [3–7].

It should be mentioned that according to the equilibrium diagram of the systems of titanium with nitrogen, oxygen and carbon, increase of the concentration of these elements greatly increases the melting point of titanium [8]. For example, the melting point of α-titanium at the mass fraction of oxygen of 3.2% is 1720°C, and at 10% it is

1885°C. The temperature of congruent melting of titanium dioxide, containing 40 wt.% of oxygen, is 1870°C.

In melting titanium ingots using different methods, the superheating of the melt above the melting point of titanium (1670°C) in the holding time of the metal in the liquid state are limited and, consequently, there is no removal of the LDI inclusions by melting [2].

Physical model

The mechanisms and relationships governing the processes of dissolution of nitrogen-containing LDI inclusions were investigated previously [4–6,9]. The aim of the present work is the examination, by the methods of mathematical modelling, of the relationships governing the dissolution of oxygen-containing refractory inclusions in the titanium melt.

The mechanism of dissolution of the oxygen-containing LDI inclusions is identical with that for the nitrogen-saturated inclusions. When an oxygen-containing low-density inclusion falls into the melt, oxygen diffuses from the inclusion into the melt since the oxygen content of the titanium melt is not high and, according to the requirements, it does not exceed 0.25%.
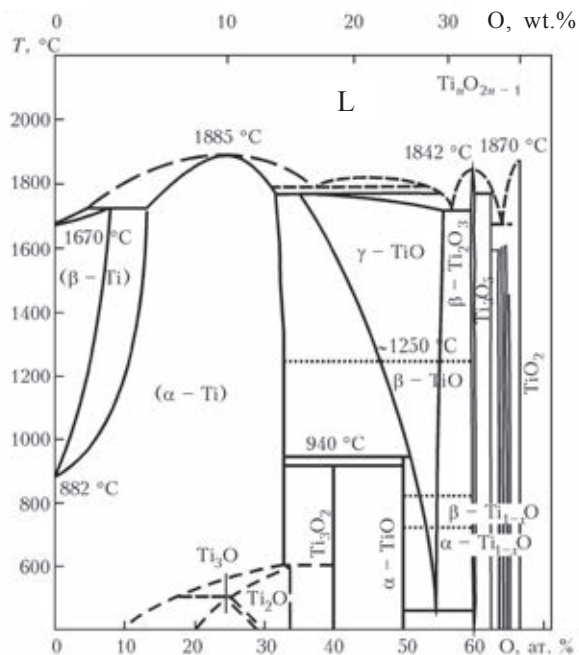

Fig. 1. Equilibium diagram of the titanium–oxygen system.

As a result of diffusion, the oxygen concentration in the surface layers of the inclusion starts to decrease. In this case, according to the equilibrium diagram (Fig. 1), the equilibrium temperature of dissolution of α-titanium at melts temperatures higher than 1720°C increases from 1855 to 1720°C with a decrease of the oxygen concentration from 10.0 to 5.3%, and when the melt temperature is lower than 1720°C and the mass fraction of oxygen is smaller than 3.2%, α-titanium transforms into β-titanium whose melting point is lower than that of α-titanium.

Thus, the process of dissolution of the inclusion may be described as follows. After transfer of the inclusion into the titanium melt, oxygen atoms stacked removed from the surface of the inclusion into the melt and during passage through the boundary diffusion field they are carried into the volume of liquid metal by convective flows.

New atoms diffuse from the volume of the inclusion to the area of the oxygen atoms which left the surface. The oxygen content of the subsurface layers of the inclusion decreases. When the concentration of oxygen in the surface layer of the solid particle becomes lower than at the appropriate liquidus line at the given temperature, the layer dissolves and the size of the inclusions decreases.

Mathematical model

To simplify the calculations, it is assumed that the particles of the oxygen-containing LDI, placing the titanium melt, is spherical with the radius R_{in} and its temperature is equal to the melt temperature T_{in}. In this case, the equation of diffusion of oxygen into the inclusion in the spherical coordinate system has the form:

$$\frac{\partial C_O}{\partial \tau} = \frac{1}{r^2} \frac{\partial}{\partial r} \left(D_O r^2 \frac{\partial C_O}{\partial \tau} \right), \tag{1}$$

where r is the actual radius in the range from 0 to R_{in}, m; $C_O = C_O (r, \tau)$ is the mass fraction of oxygen in the inclusion, %; $D_O = D_O (C_O)$ is the coefficient of oxygen diffusion in

the solid particle, m^2/s; is the time from the start of the dissolution process, s.

The boundary condition in the centre of the particle is determined by the symmetry conditions

$$\frac{\partial C_O}{\partial r}\Big|_{r=0} = 0. \tag{2}$$

Since after passage through the boundary diffusion layer in the melt, the oxygen atoms are transferred into the volume of liquid metal by the convective flows, the boundary condition on the surface of the inclusion has the following form:

$$-D_O \frac{\partial C_O}{\partial r}\Big|_{r=R_{in}} = \beta_O \left(C\big|_{r=R_{in}} - LC_O^L \right), \tag{3}$$

where β_O is the coefficient of mass transfer of oxygen in the titanium melt, m/s; L is the equilibrium coefficient of distribution of oxygen between the solid and liquid phases; C_O^L is the mass fraction of oxygen in the volume of the melt, %. In the first approximation, the coefficient of distribution of oxygen between the phases L can be assumed to be equal to 1.5 and constant [10].

The initial distribution of the oxygen concentration in the volume of the inclusion is also assumed to be constant:

$$C_O(r,0) = C_{in}. \tag{4}$$

The numerical solution of the mathematical model of dissolution of the oxygen-containing inclusions in titanium is obtained using the Cranck–Nicholson finite-difference method [11]. Equation (1) is approximated on the basis of the implicit 6-point template which ensures the unconditional stability and convergence of the numerical solution.

The process of dissolution of the inclusion in the programme was realises taking into account analysis of the values of concentration after everytime step and reduction of the working sample by the number of the points in which the mass fraction of oxygen is lower

than the concentration corresponding to the liquidus line at the calculation temperature.

In the determination of the diffusion coefficient of oxygen in titanium it must be taken into account that its value depends strongly on the form of the crystal lattice of titanium. Since diffusion is an activation process, the temperature dependences of the diffusion coefficients can be expressed in the exponential form. Averaging of the results of the experimental investigations concerned with the determination of the oxygen diffusion coefficient in titanium [10–12] gave the following temperature relationships:

$$D_O^\alpha = 3.45 \exp\left\{ -\frac{211901}{RT} \right\}, \tag{5}$$

$$D_O^\beta = 0.89 \exp\left\{ -\frac{173861}{RT} \right\}. \tag{6}$$

According to the results of experimental investigations, published in [13, 14], the temperature dependence of the diffusion coefficient of oxygen in the titanium dioxide has the following form:

$$D_O^\gamma = 1.1 \exp\left\{ -\frac{305870}{RT} \right\}. \tag{7}$$

In the programme, realising the numerical solution of the mathematical model (1)–(4), the diffusion coefficient was determined at every point on the basis of the oxygen content in the same point in the previous time step, i.e., at the given calculation temperature and the computed concentration of oxygen the equilibrium diagram was used to determine the phase composition of titanium and, subsequently, the equations (5), (6) or (7), respectively, were used to calculate the value of the diffusion coefficient. It was assumed that in the two-phase zones, for example α+β, the diffusion coefficient changes in a linear manner with the decrease of the concentration from respectively D_o^α to D_o^β.

The calculations carried out in [9] for the

numerical value of the coefficient of mass transfer of oxygen in the titanium melt gave the estimate $\beta_O = 0.01$ cm/s.

Relationships governing the dissolution of oxygen-containing inclusions

The investigations of the dynamics of distribution of oxygen in the volume of the inclusion using the mathematical model (1)–(4) shows that the nature of dissolution of the oxygen-saturated particle of α-titanium greatly depends on the melt temperature.

At a temperature of 2000 K the oxygen concentration in the entire volume of the inclusion is constant, with the exception of a narrow layer and the phase boundary, and the subsurface layer with a thickness of 15-20 μm showed a large reduction of the mass fraction of oxygen from its initial value to the concentration corresponding to the AC1 line (liquidus line) at the given temperature (Fig. 2a).

With time, the outer layers of the inclusion dissolve (with low oxygen content) and the concentration gradient is displaced with dissolution of the particle to the centre of the inclusion together with the phase boundary.

At a temperature of 1950 K, the oxygen content decreases throughout the entire volume of the inclusion, and the size of the inclusion changes only slightly in the initial stage of dissolution (Fig. 2b).

Analysis of the dependence of the radius of the oxygen-containing inclusions on holding time in the melt (Fig. 3) shows that at a temperature of 2000 K the particles of α-titanium dissolve at an almost constant rate (the speed of displacement of the interface is approximately 28 μm/s), whereas the rate of dissolution of this particle at a temperature of 1950 K is highly non-linear: in the initial stage, the dimensions of the inclusions remain almost completely constant and then starts to decrease with increasing rate up to complete dissolution.

The constructed mathematical model (1)–(4) can be used to determine the relationships of the removal of oxygen-containing
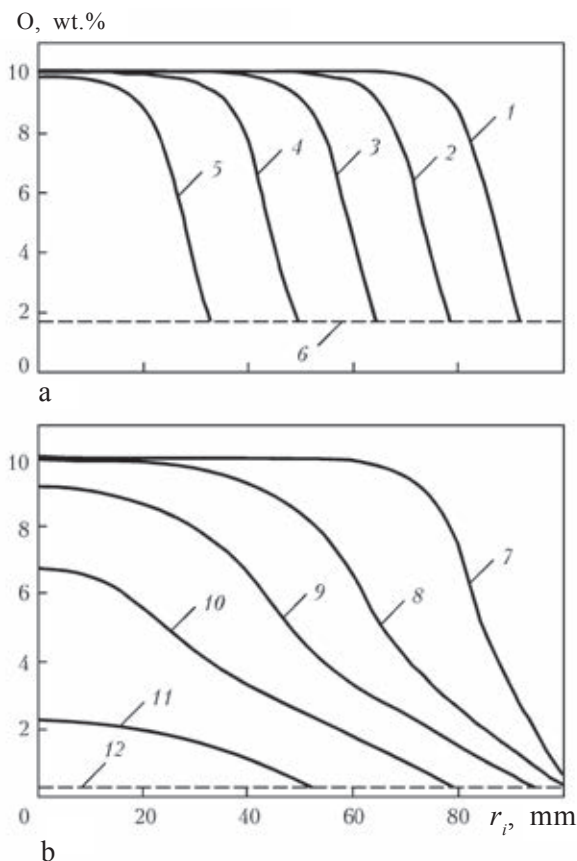

Fig. 2. Distribution of the oxygen concentration in the particle of α-titanium in relation to time at a temperature of 2000 (a) and 1950 K (b), s: 1) 6; 2) 12; 3) 18; 4) 24; 5) 30; 6) AC1 = 1.69%; 7) 12; 8) 42; 9) 72; 10) 102; 11) 132; 12) AC1 = 0.256%; r_i is the radius of the inclusion.

inclusions from titanium and its alloys in different remelting processes in special electrometallurgy by plotting the dependence of the time to complete dissolution of the inclusion on the melt temperature for solid particles with different chemical composition and dimensions.

The effect of the temperature of liquid titanium on the dissolution time of the oxygen-containing inclusions is very strong. With increase of temperature the period of existence of the inclusion in the melt rapidly decreases (Fig. 4). For example, for a α-titanium particle with a diameter of 2 mm, the increase of superheating of the melt by 100 K (from 1950 to 2050 K) reduces the dissolution time of the inclusion by more than a factor of 4, i.e. from 150 to 36 s.
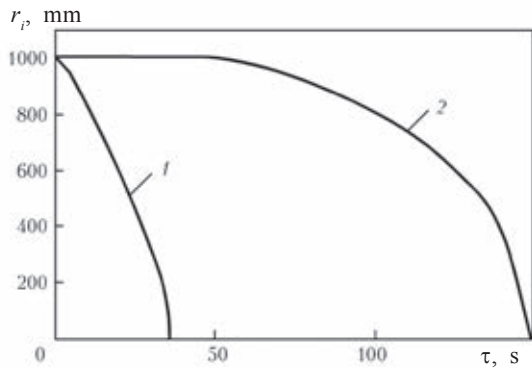
Fig. 3. Dependence of the radius of the α-titanium inclusion on holding time τ in the melt at a temperature of, K: 1) 1950; 2) 2000.
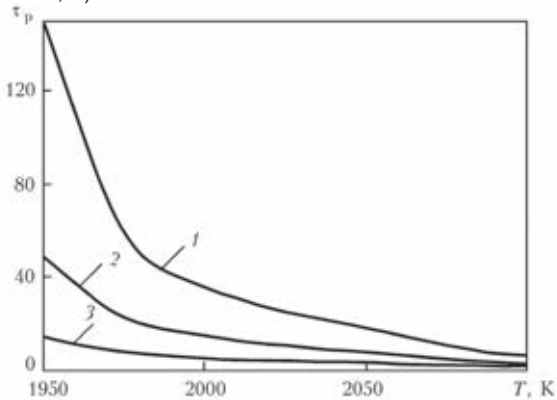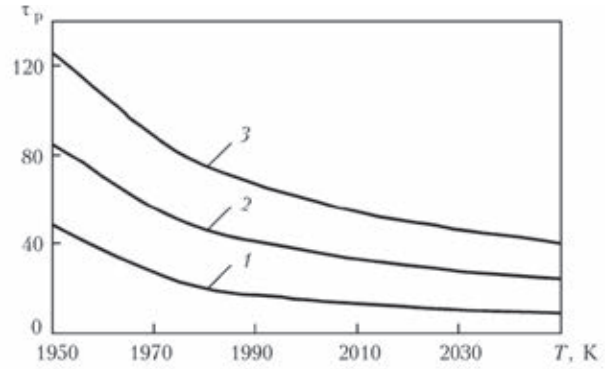

Fig. 5. Dependence of the dissolution time of the oxygen-containing inclusions on temperature at different initial mass fraction of oxygen in the inclusion, %: 1) 10; 2) 25; 3) 40.
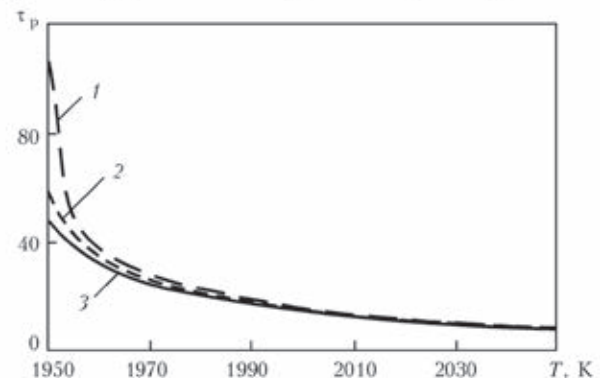

Fig. 4. Dependence of dissolution time τ_p of the particle of the α-titanium on temperature at a different sizes of the inclusion, mm: 1) 2; 2) 1; 3) 0.5.

Fig. 6. Dependence of the dissolution time of the particle α-titanium on the temperature at different mass fractions of oxygen in the melt, %: 1) 0.17; 2) 0.12; 3) 0.06.

At a temperature of approximately 1990 K, the curves of the dependence of the dissolution time of the oxygen containing particles shows and inflection point, i.e., at temperatures lower than 1990 K the rate of decrease of the duration of existence of the inclusion in the melt of titanium with increasing temperature is approximately twice the value at a temperature greater than 1990 K. This dynamics of the variation of the size of the inclusions is determined by the differences in the nature of distribution of oxygen in the volume of the inclusion during dissolution which was determined seriously by the methods of mathematical modelling (Fig. 2).

The dependence of the duration of existence of the inclusion in the melt on its linear dimensions is almost completely linear (Fig. 4). In superheating the titanium melt by more than 150 K the increase of the decrease of the diameter of the inclusion by a factor

of 2 correspondingly increases only uses the dissolution time by a factor of 2, and when the melt is superheated by more than 150 K – up to 3 times.

With increasing initial oxygen concentration in the particle, the rate of dissolution of the particle decreases and the duration of complete dissolution increases (Fig. 5). This is caused by the fact that the coefficient of diffusion of oxygen in the titanium dioxide is considerably lower than that in α-titanium.

For example, at a temperature of 1950 K the coefficient of diffusion of oxygen in titanium is equal to $8.55 \cdot 10^{-6}$ cm/s, and in the titanium dioxide it is $8.86 \cdot 10^{-9}$ cm/s. Therefore, the inclusions of α-titanium, saturated with oxygen, dissolve in the titanium melt at a rate of 2.5 or more times greater than the rate of dissolution of the titanium dioxide inclusions.

The oxygen concentration in the titanium

melt has only a slight effect on the dissolution time of the inclusion (Fig. 6), with the exception of slight superheating of the melt above the melting point of titanium. In the latter case, the equilibrium oxygen concentration on the surface of the solid particle may approach even exceed that of oxygen on the AC1 line of the equilibrium diagram of the titanium–oxygen system (liquidus line). The dissolution time of the inclusion greatly increases, and the process of dissolution of the inclusion may even be arrested.

Conclusions

1. The mechanism has been proposed and a mathematical model of the process of dissolution of the oxygen-containing titanium inclusions (α-containing particle or titanium dioxide) in liquid titanium was constructed. The model can be used to calculate the rate of dissolution of the particle in the melt.

2. Differences in the dynamics of distribution of oxygen in the particles of α-titanium in the process of dissolution in superheating the melt above the melting point of titanium (higher or lower than 150 K) were determined.

3. The duration of complete dissolution of the oxygen-containing inclusions in relation to the chemical composition and initial dimensions of the inclusions was determined.

References

1. Henry J.L., et al., Metal Transactions, 1973, No. 4, 1859-1864.
2. Bakich R., The Journal of Metals, 1991, volume 43, 42-44.
3. Paton B.E., et al., Electron beam on melting of refractory and high-reactivity metals, Naukova Dumka, Kiev, 2008.
4. Bellot J.P. and Mitchell A., Light Metals, 1994, No. 2, 1187-1193.
5. Jarrett R.N., et al., Proceedings of the Six World Conference on titanium, Les Editions de Physique, France, 1988, 393-398.
6. Jarrett R.N., et al., Proceedings of the conference on electron beam melting and refining - state of the arc, New Jersey, 1986, 332-346.
7. Tripp D.W., et al., ibid, 1986, 30-44.
8. Hansen M. and Anderko K., Structures of binary alloys, Metallurgizdat, Moscow, 1986.
9. Akhonin S.V., Probl. Spets. Elektrometall.2001, No. 1, 20-24.
10. Amelin A.N., Sovremennaya Elektrometallurgiya, 2009, No. 4, 20-24.
11. Marchuk G.I., Methods of computing mathematics, Nauka, Moscow, 1980.
12. Kogan Ya.D., et al., Constants of interaction of metals with gases, handbook, Metallurgiya, Moscow, 1987.
13. Belova S.B., et al., Tsvetn. Metall., 2000, No. 4, 33-37.
14. Decham M., et al., Titanium: Physical metallurgy and technology, The proceedings of the Third International conference for titanium, volume 2, Moscow, 1976, 159-168.
15. Kofstad P., High-temperature oxidation of metals, John Wiley and Sons, New York, 1966, 169-178.
16. Simon D., et al., In: Titanium: Physical metallurgy and technology, proceedings of the Third International conference on titanium, Moscow, 1976, 169-176.

Effect of the surface curvature of the substrate on the structure and properties of thermal barrier condensed coatings

K.Yu. Yakovchuk, Yu.E. Rudoi, L.M. Nerodenko, E.V. Onoprienko and A.O. Akhtyrskii

E.O. Paton Electric Welding Institute, Kiev;
Research Institute for Electron Beam Technologies, E.O. Paton Electric Welding Institute, Kiev

Abstract: The results of investigations of the chemical composition, structure and some properties of thermal barrier gradient coatings produced by electron beam evaporation of composite ceramic ingots on the base of zirconium dioxide to the surface of heat-resistant alloys using a single-stage technology are presented. The method of deposition of thermal barrier coatings on samples in equipment, simulating the conditions of condensation on areas of gas turbine blade airfoils with positive and negative curvatures of the surface (in the area of convex and concave sides) is described. The effect of temperature of coatings deposition on their structure and properties (microhardness, porosity and thermal cycling life) was established. A positive effect is shown by application of treatment of external ceramic layer by argon ions during the process of deposition, as well as by a gradient adding of gadolinium oxide into its composition to prevent the appearance of microstructural defects in the form of microcracks and to improve the thermocyclic life of coatings in the concave area of concave side.

Thermal barrier coatings are used for increasing the service life of working and nozzle blades of gas turbine engines (GTE) as a result of protecting the substrate (the blade metal is a creep-resisting alloy based on nickel or cobalt) against the thermal, oxidation and corrosive effect of the products of combustion of fuel [1–3]. In addition to extending the service life and reducing the frequency of servicing and production costs, the thermal barrier coatings improve the efficiency of operation of the duty as a result of increasing the temperature of the gas at the inlet into the hot circuit of the turbine.

The thermal barrier coatings are a multilayer structure with an internal metallic heat-resisting layer based on MCrAlY (M – Ni, Co) or intermetallic compounds NiAl, CoAl, PtAl and an external ceramic layer with low heat conductivity, usually based on partially stabilised zirconia ZrO_2–8%Y_2O_3 (YSZ), and also and aluminium oxide interlayer bonding the external and internal layers.

In [7–9] the authors describe single-stage electron beam technology of depositing gradient thermal barrier coatings in which the binding metallic layer, transition zones and the external ceramic layers are deposited by evaporating the composite ceramic ingot from a single source of a carousel evaporator in a single vacuum cycle. This improves the service characteristics of the thermal barrier coating, primarily is thermal cyclic longevity, and also greatly simplifies the process of deposition and reduces the time/expenditure required for depositing the coating.

The structure of the external ceramic layer, formed in condensation from the vapour phase, is determined by various parameters such as the substrate temperature in the deposition, the angle of incidence of the vapour flow, the pressure in the working chamber, the rate of deposition of the coating [10–13].

An increase of the angle of incidence of the vapour flow on the condensation surface reduces the microhardness and susceptibility to brittle fracture of the ceramic coating and porosity increases.

The curvature of the surface on which the coatings deposited is an important parameter [14]. The profile of the blade is complicated and characterised by the presence of both convex (back, inlet and output edge) and concave (trough) sections. The structure and properties of the individual sections of the profile of the ceramic layer deposited in a single cycle differ [15].

The aim of the present work is the investigation of the structure and some properties of the gradient thermal barrier coating in relation to profile of the substrate surface and the parameters of the deposition process. It is attempted to develop a simulation procedure of the position of the external ceramic layer which would reflect the conditions of formation of the coating on various sections of the blade (in particular on the back and the trough) and relate the microhardness, porosity and thermal cyclic longevity of this coating with its microstructure.

Experimental material and procedure

The gradient thermal barrier coating was deposited by electron beam evaporation of a composite ceramic ingot followed by condensation of the vapour phase on the surface of the specimens in a single vacuum cycle of deposition by the technology described in [9]. The coating consisted of a three-layer structure with the internal binding layer based on the Ni–18% Co–18% Cr–11% Al–0.2% Y alloy (here and in the rest of the article, the content of the elements is given in wt.%), the transition zone based on nickel aluminide
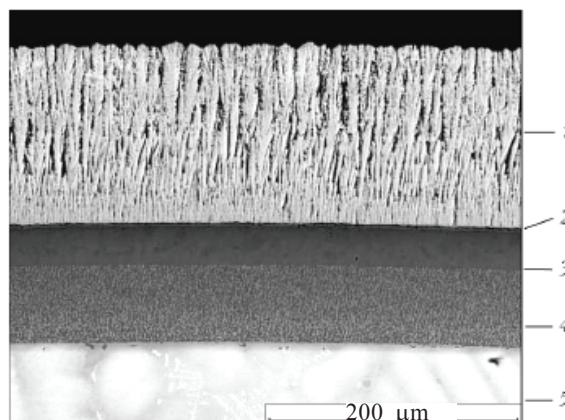

Fig. 1. The microstructure of the gradient thermal barrier coating produced by electron beam evaporation and condensation in vacuum (the region of the back section, Tc = 850°C): 1) ZrO2-8%Y$_2$O$_3$ ceramic layer; 2) TGO; 3) the NiAl-Cr transition zone; 4) SDP-1; 5) ZhS-32VI creep resisting alloy.

NiAl with the gradient variation of the chromium content, and the external layer based on partially stabilised zirconia ZrO_2–8% Y_2O_3 (Fig. 1).

The internal binding layer was deposited by evaporating an ingot of NiCoCrAlO alloy. The transition zone based on nickel aluminide with the additions of chromium and the external ceramic layer were produced by gradual evaporation of a tablet of AlCr situated in the upper part of the composite ceramic ingot ZrO_2–8%Y_2O_3, followed by complete evaporation of the ingot [9].

The structure of the external ceramic layer in some experiments was modified by treating the condensate surface with argon ions during deposition.

In one of the experiments, a thermal barrier coating was also deposited on the specimen with the coating containing also approximately 25% of gadolinium oxide (Gd_2O_3), added in the gradient manner into the outer ceramic layer. For this purpose, a tablet of Gd_2O_3 was pressed into the lower part of the composite ceramic ingot [16].

It should be mentioned that the technological parameters in all experiments with the deposition of the gradient coatings were constant, with the exception of the deposition temperature T_d of the ZrO_2–8% Y_2O_3 layer, and equalled 600, 850 and 1000°C at

a deposition rate of 5–6 µm/min. Prior to depositing the coating, the working surface of the specimens was ground with abrasive paper to the surface finish grade corresponding to R_a = 0.1–0.5 µm.

The conditions of condensation of the coating in individual parts of the blade were modelled using as the main element of equipment a bent substrate 5 mm thick of Cr18Ni10Ti steel in the form of a sector with a radius of 18 mm (placed on the rotating shaft above the evaporated ingot in the electron beam equipment). Flat specimens with a diameter of 14 mm and 4 mm thick, produced from ZhS-32VI creep-resisting alloy (Fig. 2) were placed on the substrate on the concave and convex sides.

The specimen, secured on the convex side of the substrate shows the formation of the structure of the coating identical with that of the back section, and on the concave side with the structure of the trough. This distribution of the substrate is made it possible, in the conditions of the single experiment, to obtain data on the structure of the external ceramic layer on the simulation flat specimens in different conditions of the formation of the vapour flow and carry out subsequently thermal cyclic comparative tests. The temperature of the specimens in deposition of the coatings was inspected using a chromel–alumel thermocouple placed inside the substrate.

After deposition a gradient thermal barrier coating, the specimens were annealed in vacuum at a temperature of 1100°C for 1 h for the formation of a thin film based on Al_2O_3 on the metal–ceramics boundary (the so-called TGO – thermally grown oxide) ensuring adhesion bonding of the metallic binder and the ceramic layers based on zirconia.

The thermal stability of the coatings was determined in isothermal oxidation of the specimens in air at 1200°C for 10 h, and the heat resistance of the coatings was investigated by furnace thermal cyclic test in air in the conditions (50↔1150°C) was holding at the maximum temperature for 45 min and the total duration of the single cycle of 60 min.

The total number of the cycles in 24 hours was 20. The moment of complete failure of the thermal barrier coating was regarded as the moment of cleavage of the ceramic layer from 25% of the surface of the specimens.

The structure of the thermal barrier coating was investigated using a CamScan 4D scanning electron microscope. The composition of the deposited layers was determined using an EDX attachment INCA-200 to the scanning electron microscope. The microhardness of the external ceramic layer was measured in equipment Micro-Droat 4000A using a standard diamond Vickers indentor with a load of 0.29 N (50g) with the fixed loading rate and holding time under load. The general porosity of the external ceramic layer was determined by the numerical methods of analysis of the microstructure of the cross-section of the condensate. Calculations were carried out using Image Pro Plus computer program based on the identification of the contrast of the investigated structure.

Experimental results

One of the special features of the formation of the gradient thermal barrier coating in deposition, in accordance with the scheme shown in Fig. 2, is the difference in the thickness of the coating in the specimens positioned in different zones simulating the profile of the blades – back and trough (Table 1). The thickness of all layers of the coating is considerably smaller on the specimens situated in the zone of the trough, in comparison with the zone of the back section of the blade, as a result of the effect of screening of the specimens, i.e., the shorter holding time directly in the zone of the vapour flow.

Figure 3 shows the distribution of the main alloying elements in the thickness of the gradient thermal barrier coating in the condition after condensation and subsequent vacuum annealing (the specimens in deposition in the zone simulating the back section). This distribution is characteristic of all the experiments because the binding metallic layer was produced at a constant temperature of
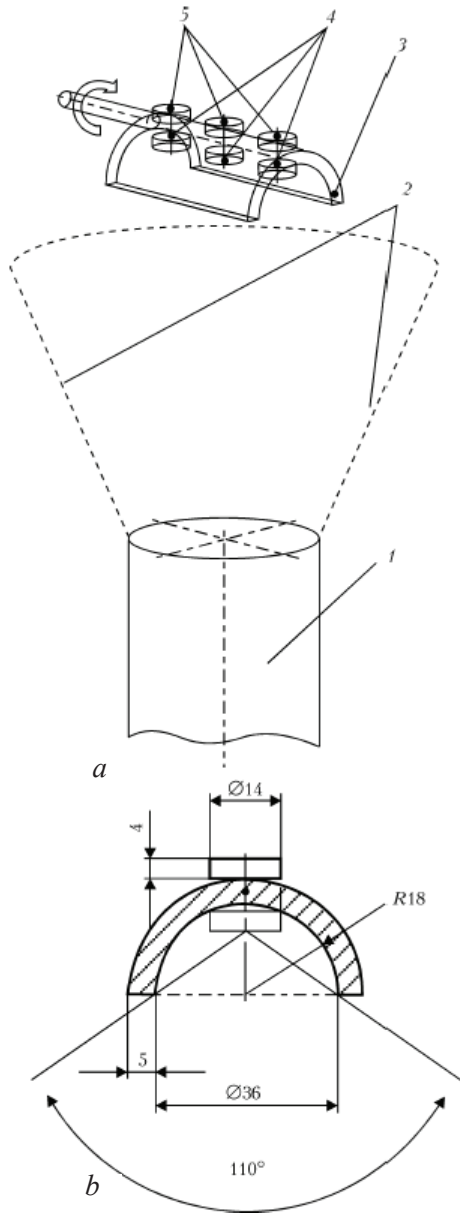
Table 1. The thickness of the metallic binder and the outer ceramic layer in the sections of the blade profile, µm

Substrate temperature in deposition of $ZrO_2Y_2O_3$ layer	Type of layer	Back section	Trough
600	Binding (NiCoCrAlY/ NiAl)	94	68
	External ceramic $(ZrO_2(Y_2O_3))$	172	118
800	Binding (NiCoCrAlY/ NiAl)	82	58
	External ceramic $(ZrO_2(Y_2O_3))$	154	108
1000	Binding (NiCoCrAlY/ NiAl)	81	57
	External ceramic $(ZrO_2(Y_2O_3))$	158	106

Fig. 2. The distribution of the specimens in equipment above the evaporated ingot (a) and the geometrical dimensions of equipment with the specimens (b): 1) the evaporating ingot; 2) the vapour flow of the deposited coating; 3) equipment; 4) specimens in the zone simulating the trough section of the blade; 5) the specimens positions in the zone simulating the of the blade.
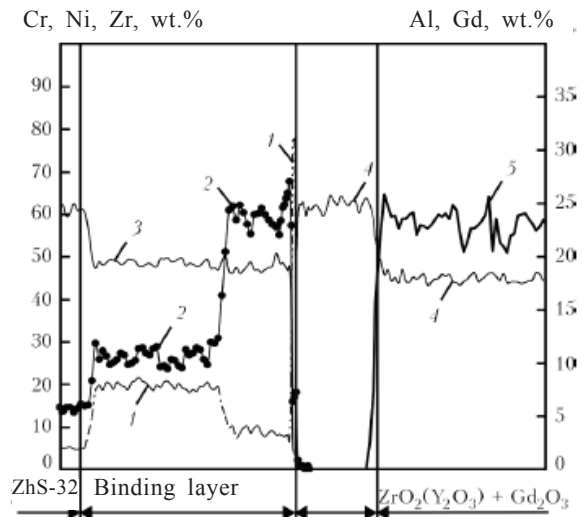

Fig. 3. Distribution of the alloying elements in the cross-section of the thermal barrier coating (the back section, deposition temperature 850°C, the condition after vacuum heat treatment at 1100°C, 1h): 1) Cr; 2) Al; 3) Ni; 4) Zr; 5) Gd.

850°C. The graph also shows the distribution of the content of the gadolinium oxide, introduced by the gradient procedure into the outer layer of the ceramic coating.

The condensation temperature of the external ceramic layer ZrO_2–8%Y_2O_3 influences primarily the behavioural nickel at the binding layer–ceramics interface (the distribution of the main alloying elements of the coating is shown in Fig. 4 for the condensation temperatures of the external ceramic layers of 600, 850 and 1000°C).

The experimental results show that the increase of the deposition temperature of the ZrO_2–8%Y_2O_3 layer increases the nickel content and results in the formation of a peak at the interface (at T_c = 1000°C). The
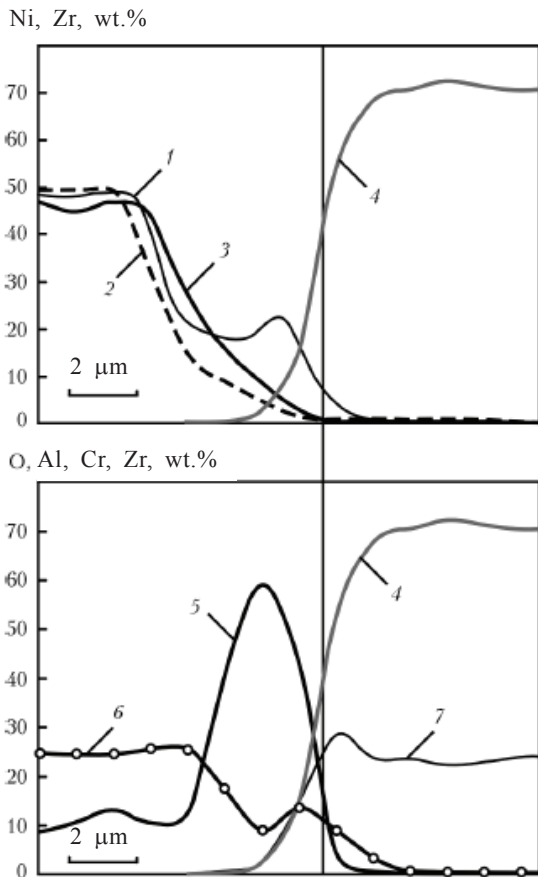
Ni, Zr, wt.%

O, Al, Cr, Zr, wt.%

Fig. 4. Characteristic distribution of the alloying elements at the binding layer (NiAl)Cr-ZrO2-8%Y_2O_3 ceramics at different values of the deposition temperature of the ceramic layer (after vacuum annealing 1100°C, 1 h), °C: 1) Ni, 1000; 2) Ni, 600; 3) Ni 850; 4) Zr; 5) Cr; 6) Al; 7) O.

position of the nickel peak coincides with the concentration peak of aluminium which in turn indicates the formation of the Al_2O_3 film.

It should be mentioned that the peak on the distribution curves of the elements in the investigated zones of the trugh also appears at T_c = 850°C. The presence of a similar nickel peak maybe associated with the formation during annealing of the nickel oxide or a spinel in the Ni–Al–O system, and not α-Al_2O_3.

Figure 5 shows the structure of the cross-section of the ZrO_2–8%Y_2O_3 external ceramic layer deposited at temperatures of 600, 850 and 1000°C. The columnar structure of the crystals, directed normal to the condensation surface, was found in the coatings of all the variants in the zone of both the back section and the trough.

The width of a single crystal increases with increase of the condensation temperatures and in the region of the trough is 1–2 μm in the temperature range 600–1000°C, and in the back region 2 μm at 600°C and approximately 5–6 μm at 850 and 1000°C. The width of the intercrystalline pores in the external ceramic layer ZrO_2–8%Y_2O_3, deposited on the specimens simulating the convex surface also increases from 1 to 3–4 μm when the condensation temperature increases from 600 to 1000°C.

Evidently, the width of the intercrystalline porosity in the trough section of the blade is almost completely independent of T_c and does not exceed 0.5 μm. The characteristic feature of the ZrO_2–8%Y_2O_3 crystal deposited at T_c = 600°C is the developed intracrystalline porosity which degenerates into single pores with increase of the condensation temperature directed along the condensation axis.

Figure 6 shows the structure of the cross-section of the ceramic layer deposited at 850°C and modified by alloying the external layers with the Gd oxide, and also by treatment with the argon ion flux during deposition. The nature of the structure in both variants is identical with the structure of the non-modified coating, deposited at T_c = 850°C. However, it should be mentioned that the width of the single crystal of ZrO_2–8%Y_2O_3, treated with the argon ions during formation of the coating, decreases to 3–4 μm in the region of the back part of the blade, and when Gd_2O_3 is added it increases to 10 μm, in comparison with 5–6 μm in the variant without modification. In the trough section of the blade there are no large differences in the structure of the ceramic layer.

An important parameter characterising the condition of the external ceramic layer in the zone of the back part and the trough section of the blade is microhardness. Figure 2 shows the dependence of microhardness on the deposition temperature of the ZrO_2–8%Y_2O_3 layer. It may be seen that the microhardness values differ considerably for the zones of the back 0part and the trough section of the blades, i.e., by a factor of 2.0–2.2.
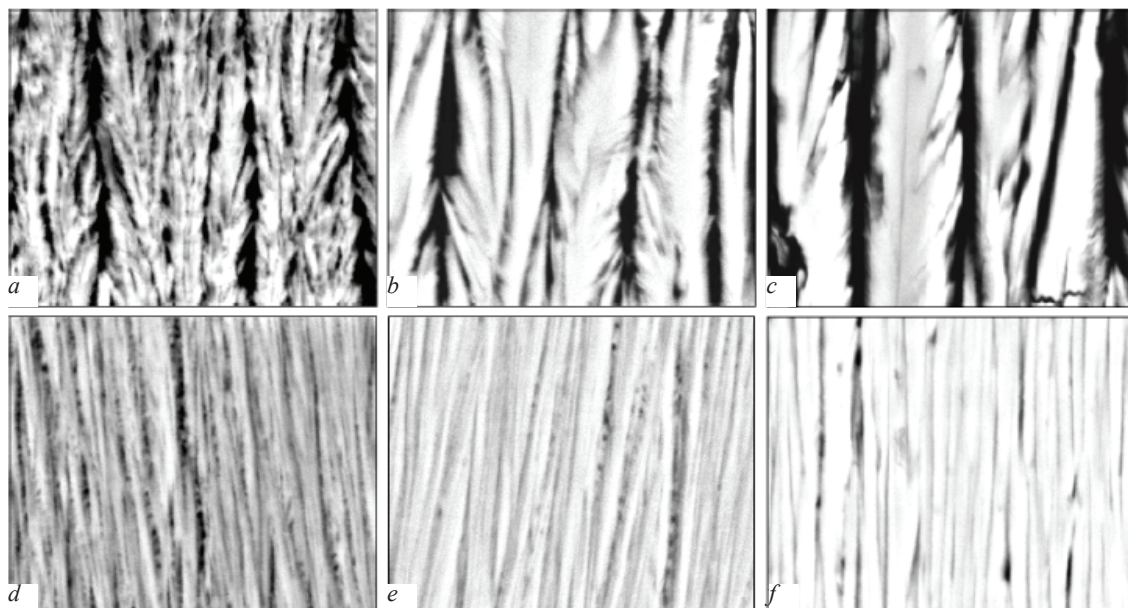
Fig. 5. The structure of the cross-section of the ZrO_2 (Y_2O_3) ceramic layer in the back section (a–c) and in the trough (d–f) in the condition after deposition; condensation temperature T_c = 600 (a, d), 850 (b, e) and 1000 (c, f), °C; × 2500.

This condition remains both in the condition after deposition and after heat treatment in vacuum or air. The large difference in the microhardness values indicates differences in the density of the ceramics in different areas of the profile of the blade and is confirmed by the results of metallographic investigation.

The lowest microhardness values in the

Fig. 6. The structure of the cross-section of the modified ceramic layer in the back section (a, b) and the trough (c, d) in the condition after deposition; a, c) modification by adding the gadolinium oxide to the external part of ZrO_2 (Y_2O_3); b, d) treatment with the argon ions during formation of the coating; T_c = 850°C, ×1000.

initial condition were shown by the ceramic layer formed in the sections with different surface curvature at T_c = 600°C. However, in vacuum annealing at 1100°C and isothermal holding in air for 10h at a temperature of 1200°C intensive sintering takes place and is accompanied by fragmentation of the structure and increase of the microhardness values.

The microhardness of the ceramics, formed in the back part of the blade at T_c = 600°C, after vacuum and oxidation processes of annealing reaches the hardness of the ceramics deposited at 850°C after the same heat treatment. The increase of the condensation temperature to T_c = 1000°C, in addition to sintering and fragmentation of the structure, is accompanied by intensive diffusion of the elements from the metallic binding layer to the ceramic layer (Fig. 4).

In addition, in the internal ceramic layer, deposited on both the specimens and actual blades at high temperature, the region of the trough part of the blade contains characteristic defects in the form of compression microcracks propagating in both the normal and parallel direction to the substrate, without extending to the surface of the ceramic layer (Figure 8). Evidently, the formation of
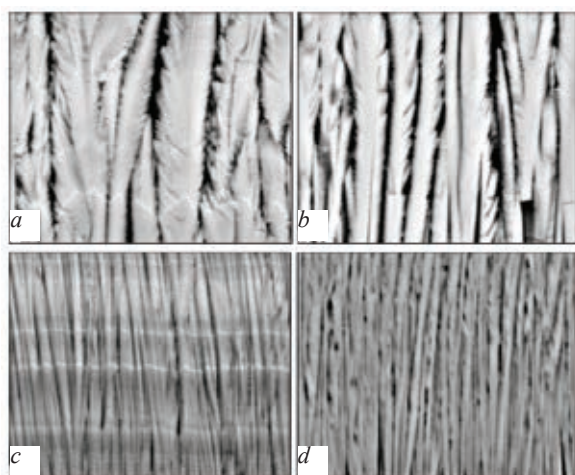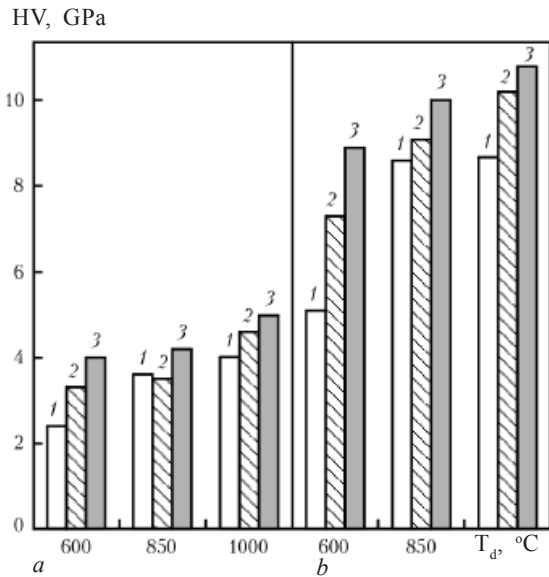
HV, GPa

Fig. 7. Effect of the deposition temperature on the micro-hardness of the ZrO_2 (Y_2O_3) layer in the initial condition and after heat treatment: a) the back section; b) the trough; 1) initial condition; 2) annealing at 1100°C, 1 h, vacuum; 3) annealing at 1200°C, 10 h, F.

Fig. 8. Examples of defects of the type of compression cracks, formed in the high-density ceramic layer with the microhardness of 9–10 GPa; a) × 250; b) × 400.

these defects is determined by the effect of the high values of the residual compressive stresses, formed in the ceramic layer, whose porosity is insufficient for relaxation of their effect. The microhardness values of the external ceramic layer in the zone of formation of these defects is no less than 9–10 GPa.

In most cases, these cracks formed in the regions of the blades (or specimens) in which the angle of incidence of the vapour flow of the deposited ceramics is close to normal, i.e., a high-density structure of the zirconia crystals forms with the minimum number of pores at a relatively low condensation rate of the ceramic layer. This also supports the formation of a high-density ceramic layer. Evidently, the most probable region of the formation of these defects is the region of the trough section of the blade.

The addition of the gadolinium oxide to the composition of the outer ceramic layer and treatment of the ceramics during sputtering with argon ions were carried out to increase the porosity of the ceramic layer reduce the susceptibility to cracking and sintering in the process of further heat treatment and service.

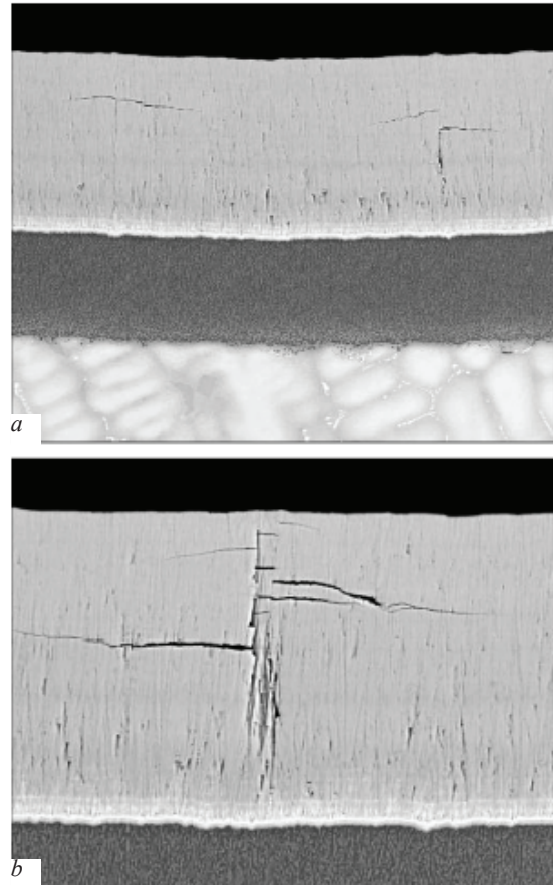Figure 9 shows the values of the microhard-ness of the ceramic layer, deposited at $T_c = 850°C$ in different conditions (after spraying, vacuum he treatment and oxidation annealing at 1200°C in air for 10 h. It can be seen that both the treatment with argon ions in the addition of Gd_2O_3 to the composition of the ceramics reduce the microhardness values in the condition after condensation, vacuum annealing at 1100°C and oxidation annealing at 1200°C, in comparison with the variant without modification.

The reduction in the density of the ceramic layer by this effect is reflected by the results of determination of porosity, presented in Table 2. The porosity values in the zone of the trough sections are considerably lower than in the back part of the blades; the increase of porosity is detected in ion treatment of the coating.

Table 2. The porosity of the outer layer (T_c = 850°C), %

Layer condition	Section of blade profile	ZrO_2–7% Y_2O_3	ZrO_2–7% Y_2O_3–Cd_2O_3	Ion treatment with Ar
Initial	Blade Trough	13.5	13.0	18.7
		5.4	5.0	10.9
Vacuum annealing at 1100°C, 1 h	Blade	16.1	15.1	23.7
	Trough	6.9	4.1	10.9
Oxidation annealing at 1200°C, 10 h	Blade	16.0	14.4	20.4
	Trough	4.3	6.3	10.9

The results of determination of longevity in thermal cycling are presented in Fig. 10. The addition of Gd_2O_3 to the external part of the ceramic layer increases the longevity of the coating at the back part of the blade but has no effect on the longevity of the coating in the trough section. Evidently, the increase of the heat resistance of the specimens, situated in the zone of the back section of the blade, is associated with the changes in the structure and heat conductivity of the ceramic layer.

Modification of the chemical composition of the ceramic material by adding zirconia and other compounds, in particular, Gd_2O_3, reduces the heat conductivity coefficient. In addition to this, one of the important parameters influencing the thermal cyclic longevity, in addition to the porosity of the coating, is the thickness of the binding metallic and external ceramic layers influencing the level of residual stresses, causing fragmentation possible separation of the ceramics during thermal cycling [17, 18]. The thicker binding layer of the coating in the region of the back section of the blade results in a stronger positive effect from modification of the coating.
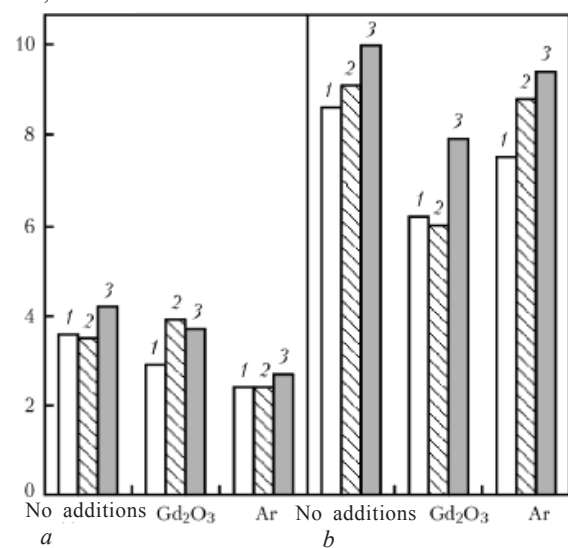
Fig. 9. Effect of modification of the ceramics by adding the gadolinium oxide and deposition with ion radiation on the microhardness of the layer of ZrO_2 (Y_2O_2) in the initial condition and after heat treatment; deposition temperature 850°C: a) the back section; b) the trough section; 1) initial condition; 2) annealing at 1100°C, 1 h, vacuum; 3) annealing at 1200°C, 10 h, F.

Fig. 10. Thermal cyclic longevity of the gradient thermal barrier coatings on the specimens in the conditions of furnace tests at 1150°C in relation to the deposition conditions of the external ceramic layer: 1) the back section; 2) the trough section; YSZ – ZrO_2–8%Y_2O_3; Gd_2O_3–ZrO2-8%Y_2O_3–Gd_2O_3; Ar– ZrO2–8%Y_2O_3 with treatment with the argon ions.

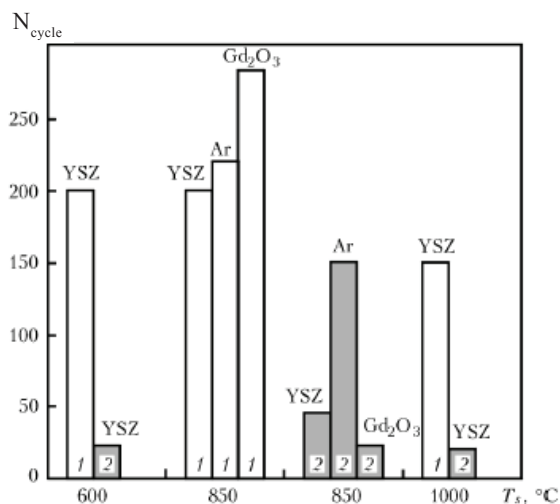Treatment of the surface of the condensate with the argon ions during formation does not change greatly the longevity of the coating in the back section but greatly increases the heat resistance of the coating in the trough section. Adhesion and heat resistance of the thermal barrier coating are determined by the properties of the interfacial surface with which these parameters are associated, i.e., the thin film of Al_2O_3. The results show that in the conditions of isothermal oxidation at 1200°C for 10 h the thickness of the Al_2O_3 film is almost independent of the deposition temperature of the ceramics and of the section of the profile (the back part, trough) and equals approximately 5–6 μm.

In thermal cyclic tests, the thickness of the TGO film (approximately 4 and 10 μm) critical for failure of the coating through the Me–TGO interface in the zones of the trough and the back section, respectively. The main reason for chipping of the external ceramic layer are the stresses formed in the TGO layer with the increase of its thickness.

The high stresses form in the coating in the sections of the blade profile with high density, in the present case in the specimens simulating the surface curvature in the trough section. If the relaxation of the stress state can take place by increasing the microhardness of the ceramic layer. Therefore, the controlling effect of ion bombardment on the condensed surface increases the porosity of the external ceramic layer in the trough section and increases the heat resistance of the coating.

Conclusions

1. The experimental results show that as a result of the 'shielding' effect, the thickness of the deposited layer of the coating in the trough section of the blade is 30–33% lower than in the back section of the blade.

2. It has been shown that the microhardness of the external ceramic layer ZrO_2–8%Y_2O_3, deposited in the trough section, is 2.2–2.5 times higher than in the back section irrespective of the deposition temperature (600, 850, and 1000°C). The level of porosity of the specimens is inversely proportional to the level of microhardness and equals 16.1 and 5.4%, respectively for the back section and the trough section at a deposition temperature of 850°C.

3. It was shown that the diameter of the single columnar crystals of ZrO_2–8%Y_2O_3, deposited in the zone of the, is 2.5–3.0 times, then in the zone of the back section.

4. The experimental results show that the ceramic layer, deposited in the trough section, with the microhardness reaching 9–10 GPa, may show the formation of specific compression microcracks propagating in the direction parallel to the substrate and not extending to the surface of the coating.

5. The results presented in the conclusions (points 1–4) are almost identical with the results obtained on the actual blades of gas turbine engines.

6. It was also found that thermal cyclic endurance of the thermal barrier coatings, deposited in the zone of the trough, is 6–8 times lower than in the zone of the back section, at the investigated the position temperatures.

7. It was shown that treatment of the external ceramic layer with the argon ions during deposition more than doubles the porosity in the zones of the cross-section, the difference in the thermal cyclic longevity of the coating in the zones of the back section in the trough does not exceed 30–35%. Ion treatment, like the addition of gadolinium oxide the ceramic layer, helps to avoid the formation of compression microcracks.

References

1. Evans A.G., et al., Progress in Materials Science, 2001, No. 4 to 6, 505-553.
2. Levi C.G., Solid State and Material Science, 2004, No. 38, 77-81.
3. Budinovskii S.A., et al., Aviats. Prom-st., 2008, No. 4, 33-37.
4. Tamarin Y., Protective coatings for turbine blades, ASM International, Ohio 2002.
5. Rhys-Jones T.N., et al., High Temperature Technology, 1989, No. 7, 73-81.
6. Schulz U., et al., Surface and Coating Technology, 2000, volume 133-134, 40-48.
7. Ukrainian patent 56228A.
8. Movchan B.A. and Yakovchuk K.Yu., Surface and Coating Technology, 2004, volume 188-189, 85-92.

9. Yakovchuk K.Yu. and Rudoi Yu.E., Sovremennaya Elektrometallurgiya, 2003, No. 2, 10-16.
10. Thornton J.A., Annual Review of Materials Science, 1977, volume 7, 239-260.
11. Novosad L.Yu., et al., Probl. Spets. Elektrometall., 1986, No. 2, 27-33.
12. Schulz U., et al., Materials Science and Engineering, 2003. Volume 360, 318-328.
13. Wada K., et al., Surface and Coating Technology, 2006, No. 200, 2725-2730.
14. Nissley D.M., Journal of Thermal Spray Technology, 1997, volume 6, No. 1, 91-98.
15. Malashenko I.S., et al., Probl. Spets. Elektrometall., 1993, No. 1, 53-65.
16. Movchan B.A. and Yakovchuk K.Yu., Materials Science Forum, 2007, volume 546-549, 1681-1688.
17. Mao w.G., et al., Mechanics of Materials, 2006, volume 38, 1118-1127.
18. Faulhaber S., et al., Journal of Mechanics and Physics of Solids, 2006, volume 54, 1004-1028.

Effect of iron concentration on the adsorptive capacity of iron oxide nanoparticles in the porous NaCl matrix in relation to atmospheric oxygen

Yu.A. Kurapov, B.A. Movchan, S.E. Litvin, G.G. Didikin and S.M. Romanenko

E.O. Paton Electric Welding Institute, Kiev

Results of investigation of the effect of iron concentration on the adsorptive capacity of nanoparticles of iron oxides to atmospheric oxygen in the porous matrix NaCl, produced from the vapor phase using electron beam evaporation and condensation in vacuum of Fe_3O_4 and iron, are given. Kinetics of the relative change of the mass of porous condensates Fe_3O_4 +NaCl and Fe+NaCl in heating up to a temperature of 650°C and air cooling was studied. It is shown that the adsorptive capacity of nanoparticles of iron oxides to atmospheric oxygen in the porous NaCl matrix increases with increase of the iron concentration in the condensate.

The nanoparticles of iron oxides and, in particular, magnetite Fe_3O_4, have been studied most extensively and are used in electronic engineering and medicine. They are used for the synthesis of magnetic liquids, transport of medical preparations, etc.

Electron beam technology of evaporation and vacuum condensation was used efficiently for the first time to produce magnetite nanoparticles. The studies [1, 2] present the results of investigation of the structure of condensates and regulation of the phase composition, structure and size of the Fe_3O_4 nanoparticles, produced by electron beam deposition of magnetite from the vapour phase. The authors of [1] investigated the possibility of producing a stabilised colloidal system with the magnetite nanoparticles with the size of 10–15 nm.

The magnetite nanoparticles, produced in the porous salt matrix, differ by high adsorptive capacity in relation to oxygen. As a result of the developed open micro- and nanosized the porosity of the salt matrix, deposited on a cold substrate, the moisture and atmospheric oxygen freely penetrate and are adsorbed on the developed open surface of the magnetite nanoparticles.

The nanoparticles of magnetite, implanted in the micro- and nanosized pores of the matrix, produced unique 'nano-reactors' of physically adsorbed oxygen and moisture. In heating in air to a temperature of the order of 380°C, the moisture and main part of the physically adsorbed oxygen are remote from the 'nano-reactors'. A further increase of annealing temperature to 650°C is accompanied by oxidation of Fe_3O_4 to Fe_2O_3 with the remaining oxygen.

Thus, the high adsorptive capacity with respect to oxygen of the Fe_3O_4+NaCl and Fe + NaCl is explained by the presence of highly active magnetite nanoparticles in oxygen. Containing the chemically bonded oxygen, the magnetite nanoparticles additionally adsorbed physically bonded oxygen from the surrounding medium. Consequently, the nanoparticles of magnetite can exist in the elementary form only in a vacuum.

In this work, investigations were carried out

into the effect of the iron concentration on the adsorptive capacity in respect of oxygen in the atmosphere of the iron oxide nanoparticles situated in the porous salt medium of the condensates Fe_3O_4+ NaCl and Fe + NaCl, produced during electron beam evaporation and subsequent condensation.

Experimental materials and procedure

The condensates were produced by the position of mixed molecular flows of magnetite and iron and NaCl sold in vacuum electron beam equipment [1, 2]. The condensation temperature was 25–45°C. The properties of the nanoparticles were investigated on the condensates and powders produced by refining in a ball mill.

The content of the elements in the condensates was investigated using a CamScan scanning electron microscope with X attachment INCA-200 Energy. The structure of the condensates in the face composition of the particles were investigated by transmission electron microscopy in a Hitachi H-800 microscope at the accelerating voltage of 100 kV. The processes of oxidation of iron in the salt matrix in air were investigated using a TGA-7 thermogravimetric analyser at temperatures of up to 650°C.

Experimental results

The results of investigations of the macrostructure and the content of the elements in the cross-section of the Fe + NaCl porous condensates show that the oxygen concentration, as in the Fe_3O_4+ NaCl condensate [2], exceeds the stoichiometric composition corresponding to Fe_3O_4 (Figure 1). The oxygen and iron content depends on the amount of iron. The amount of iron increases with increase of the content in the condensate and exceeds its value (1.33) for the stoichiometric composition Fe_3O_4. Only when the iron content of the condensate is approximately 30 at.%, when the probability of aggregation of the nanoparticles in the mixture vapour flow and in condensation on the substrate is high
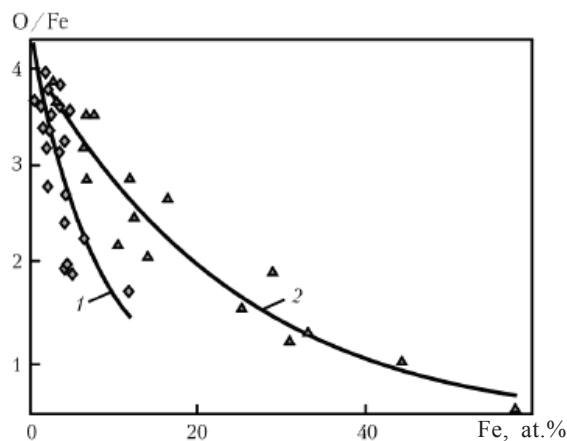

Fig. 1. The ratio of oxygen to iron in the Fe3O4+ NaCl (curve 1) and Fe + NaCl (curve 2) condensates in relation to iron content.

the content approaches the stoichiometric value (Fig. 1). This again confirms the high adsorptive capacity for oxygen of the iron nanoparticles of small dimensions [3].

Investigation by transmission electron microscopy of the thin cleavage sections of the Fe + NaCl condensate shows, as in the Fe_3O_4+NaCl condensate [2], the presence of a nanosized substance with the phase composition corresponding to magnetite (Fig. 2). This is explained by the fact that in extraction of the condensate from vacuum the atmospheric oxygen freely penetrate into the pores of the condensate and actively interacts with the developed open surface of the iron nanoparticles, implanted in the micro- and nanosized pores of the salt matrix.

In the process of separation in air of the condensate from the substrate the integrity of the condensate is disrupted and a large number of previously closed pores open,
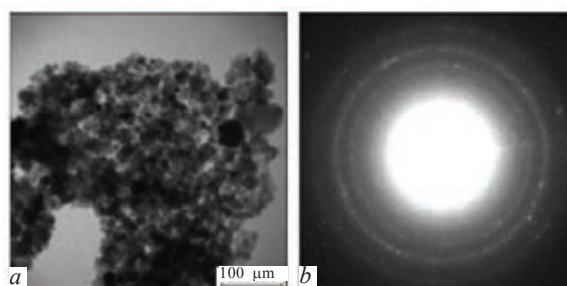

Fig. 2. Microstructure (a) and electron diffraction diagram (b) of the initial Fe + NaCl condensate.

iron is oxidised with the calorific effect accompanied by the ignition of a paper sheet on which the condensate separated from the substrate was placed.

Since the high adsorptive capacity with respect to oxygen is typical to a large extent of the small nanoparticles, this maybe evident in the thermogravimetric analysis of the kinetics in the relative variation of the mass of the porous condensates Fe_3O_4+NaCl and Fe + NaCl in heating to 650°C followed by cooling in air.

The investigations carried out on the Fe_3O_4+NaCl condensates with the iron content of 4–7 wt.% show that the increase of temperature (in heating at a rate of 10°C/min) results in all cases in a reduction of the mass of the porous condensate, down to a temperature of 380°C (Fig. 3a).

In the first stage (heating of the porous condensates to 380°C) a large fraction of the physically adsorbed oxygen is removed and this fraction increases with increase of the iron content of the condensate.

In the second stage, in further heating of the porous condensates with the magnetite nanoparticles up to a temperature of 650°C Fe_3O_2 is oxidised to Fe_2O_3 and this is carried out using the remaining fraction of the physically adsorbed oxygen [2]. Refining the ball meal of the condensate to production of the powder with the micron dimensions had no effect on the kinetics of relative variation of the mass of the given material in thermogravimetric analysis (Fig. 3b).

Similar investigations, carried out on the Fe + NaCl with the mass fraction of iron in the range 8–47% show (Fig. 3c) that the condensates with the low and medium iron content are characterised by the same dependence of the reduction of the mass of the porous condensate in the first stage in heating to 380°C and then to 650°C in the second stage.

The first stage of heating is also characterised by the removal of a large fraction of the physically adsorbed oxygen which increases when the iron content of the condensate increases (Fig. 3, curves 4 and 6).
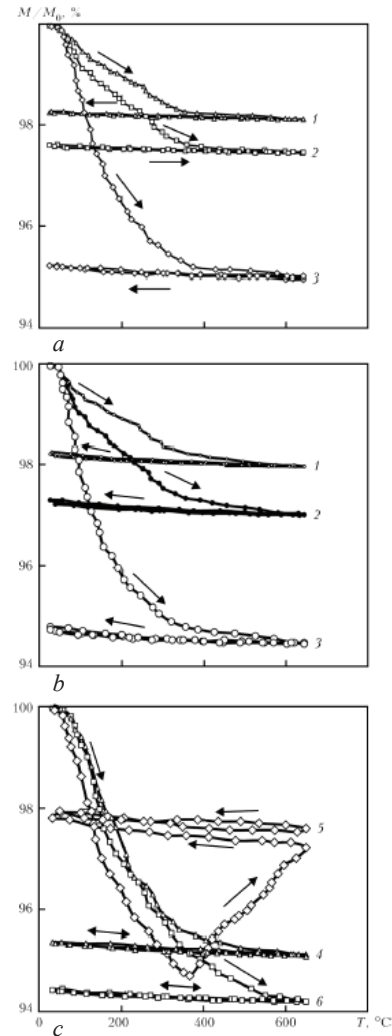
Fig. 3. The kinetics of the relative variation of the mass M/M_0 (a) and powders (b) of Fe_3O_4 + NaCl and also Fe + NaCl condensates (c) in heating and cooling in air in relation to the mass fraction of iron, %: 1) 4; 2) 5; 3) 7; 4) 8; 5) 47; 6) 20.

For the condensates with 47 wt.% of iron the shortage of physically adsorbed oxygen in the second stage is compensated by the atmospheric oxygen and, consequently, the mass of the porous condensate increases (Fig. 3, curve 5).

The effect of the amount of iron in the condensate on the ratio of the oxygen and iron content is very strong at concentrations of up to 10–15 at.% of iron (Fig. 1). With a further enquiries of the iron content of the condensate, the ratio slowly decreases.

The results of investigations of the effect of the iron concentration on the adsorptive

---

capacity of the iron oxide nanoparticles with respect to atmospheric oxygen in the porous matrix of NaCl confirmed this relationship. If in the range of low iron concentration in the fraction of the physically adsorbed oxygen rapidly increases with increase of the iron content of the condensate (Fig. 3a, b), then at high iron concentrations this fraction increases only slightly and reaches the maximum value of 5.5% (Fig. 3c).

Thus, the small iron nanoparticles, produced by molecular beam evaporation in the porous salt matrix, characterised by the high adsorptive capacity in relation to oxygen in opening the vacuum chamber. Only in the case of the high iron content in the condensate when the probability of aggregation of the nanoparticles in the mixed vapour flow and in condensation on the substrate is high, the adsorptive capacity with respect to oxygen decreases and reaches the minimum value.

References

1. Kurapov Yu.A., et al., Sovremennaya Elektrometallurgiya, 2009, No. 3, 26-28.
2. Movchan B.A., et al., Regulation of the composition and structure of the nanoparticles of the Fe-O system produced by electron beam evaporation of Fe_3O_4.
3 Serev G.B., Nanochemistry, Publishing House of the Moscow University, Moscow, 2007.
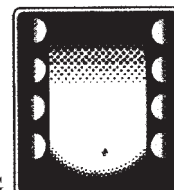
VACUUM INDUCTION MELTING

Refining of metal in melting of copper and its alloys from waste

V.N. Koleda, V.M. Ilyushenko, F.K. Biktagirov, A.V. Gnatushenko and E.P. Luk'yachenko

E.O. Paton Electric Welding Institute, Kiev

The results of investigations of refining oxidizing-deoxidizing melting of copper using a preset amount of copper oxide as an oxidizer and the calculated amount of phosphorus copper as a deoxidizer are given. A significant reduction in the hydrogen and phosphorus content in metal was found showing the positive effect on the quality of produced copper and copper-based, including weldability. It is shown that electroslag melting produces high-quality metal with a low content of gases and non-metallic inclusions from fine-dispersed wastes of copper-containing alloys.

In melting of copper and its alloys special attention is given to the problem of producing high-quality castings, especially in processing the charge containing the waste of these metals. One of the main factors which have a negative effect on the quality of melted components is the gas saturation of metal. The higher oxygen and hydrogen content in copper influences not only the density of castings but also the mechanical properties of metal and its weldability.

Hydrogen is especially harmful with respect to the formation of pores. This is explained by the fact that its solubility in the liquid copper is several times lower than in the solid copper [1–4]. Therefore, when the hydrogen content of copper is higher than 2 ppm, solidification of metal is accompanied by the release of hydrogen in the form of gas and this may lead to the formation of pores.

One of the methods of improving the quality of cast copper as a result of removal of impurities of other metals with higher affinity for oxygen is the refining of the melt by oxidation melting followed by deoxidation of metal [5].

In the first stage of this treatment it is necessary to remove of hydrogen from the metal because the equilibrium content of this element in copper decreases with increasing oxygen concentration [1].

It is interesting to investigate the effect on the gas saturation of liquid metal and produced castings of oxidation refining melting consisting of the following operations:

– oxidation of impurities;

– removal of oxides from metal;
– deoxidation of parent metal.

The oxidation process can be carried out by oxygen either as gas (from the atmosphere or specially prepared gas) or as oxygen including the composition of the oxides of the parent metal.

In the former case, it is quite difficult to control the degree of oxidation of metal and the residual oxygen content of copper. Consequently, this doesn't make it possible to determine accurately the required amount of deoxidation material. In the final analysis, the completed material may contain an excess content of hydrogen or the deoxidation element.

In the production of final products, used for the manufacture of components, to reduce the hydrogen content in the content of harmful impurities in the copper components it has been proposed to oxidise the liquid metal by adding a specific amount of copper oxide. Consequently, this makes it simple to use the calculated amount of the deoxidation agents in deoxidation of liquid metal.

To determine the effect of the melting methods on the content of hydrogen, oxygen and impurities in liquid metal and castings, comparative experiments were carried out with conventional and oxidation–deoxidation technologies.

Melting was carried out in an induction furnace with a graphite crucible. The charge was in the form of copper pigs, melted in the plant conditions by induction remelting of the copper shavings produced after machining casting components. The gas and chemical analysis of the charge materials showed that it contained 15 ppm of hydrogen, 70 ppm of oxygen and 550 ppm of phosphorus.

Copper (10 kg) was loaded into a graphite crucible together with 0.5 kg of molten borax used as the covering slag. To produce the liquid melt in each stage of fixed holding, processing of the liquid metal with the oxidation of deoxidation agents, metallic samples were taken and used for the preparation of specimens for gas and chemical analysis.

In melting by the conventional technology, copper after melting was held in the liquid state for 10 min and this was followed by deoxidation with phosphorus copper M F10. 0. 03 kg of phosphorus copper, equalling 0.03 wt.% of phosphorus, was added to each melt. After adding phosphorus copper, the melt was held for 5 min and poured into flat graphite moulds to produce castings approximately 20 mm thick.

The results of gas and chemical analysis of the charge materials, samples and castings are presented in Fig. 1. It may be seen that the mass fraction of oxygen in the liquid metal, in comparison with the oxygen content of the charge, increases and this may be explained by the dissolution in the melt of the oxides situated on the surface of the charge materials. This slightly reduce the hydrogen content of molten copper as a result of its oxidation and caused partial burning out of phosphorus. After holding the metal in the liquid state for 15 min, the hydrogen phosphorus content remains almost constant, whereas the oxygen content decreased from 120 to 100 ppm as a result of the interaction of oxygen with the carbon of the graphite crucible.

The deoxidation of liquid metal with phosphorus copper resulted in a rapid decrease of the oxygen content of molten metal, increase of its phosphorus content and a small reduction of the mass fraction of hydrogen as a result of the degassing of liquid metal in evaporation of the phosphorus oxides.

The hydrogen and phosphorus content of the castings remain the same as in the liquid metal prior to the casting, and the oxygen content slightly increase. This may be explained by a low degree of oxidation of the melt during pouring.

In melting by the oxidation–production technology, after melting copper and holding copper in the liquid state for 15 min, 0.05 kg of copper oxide was placed on the surface of the slag in the form of powder, the melt was held for 20 min and then deoxidised with 0.03 kg of phosphorus copper and poured into the mould after 5 min.

As indicated by the results presented in Fig. 2, the parameters recorded prior to addition
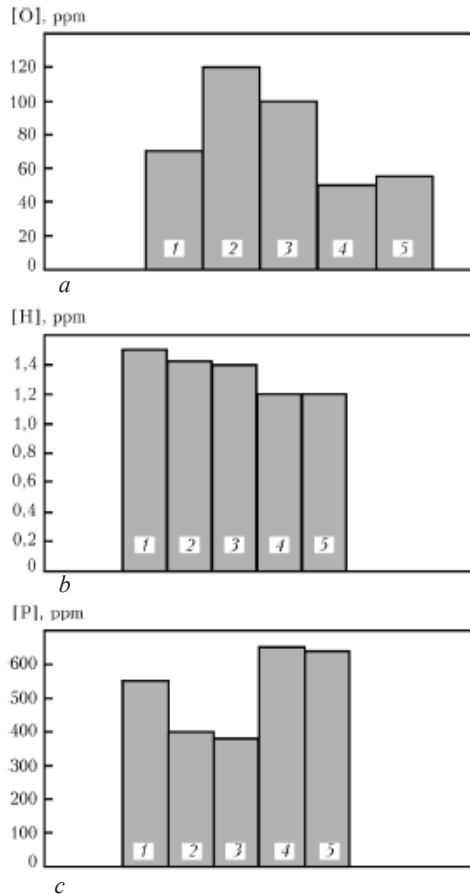
Fig. 1. Content of oxygen (a), hydrogen (b) and phosphorus (c) in charge 1, liquid metal after melting 2, holding 3, deoxidation 4 and in the casting 5; melting by conventional technology.

Fig. 2. Content of oxygen (a), hydrogen (b) and phosphorus (c) in charge 1, liquid metal after melting 2, holding 3, oxidation 4; holding 5; deoxidation 6; in the casting 7; oxidation-deoxidation melting.

of the copper oxide were almost the same as in melting by conventional technology. After adding the copper oxide to the melt the hydrogen content increased and the oxygen and phosphorus content of the liquid metal rapidly decreased.

This large decrease of the mass fraction of hydrogen can be explained by its oxidation in interaction with hydrogen and additional degassing of liquid metal in the evaporation of the phosphorus oxides.

Subsequent holding of the metal in the liquid state are resulted in a small reduction of the oxygen content. The amount of hydrogen and phosphorus was almost unchanged. Deoxidation with phosphorus copper reduced the oxygen content below the level recorded in the charge materials, and the phosphorus
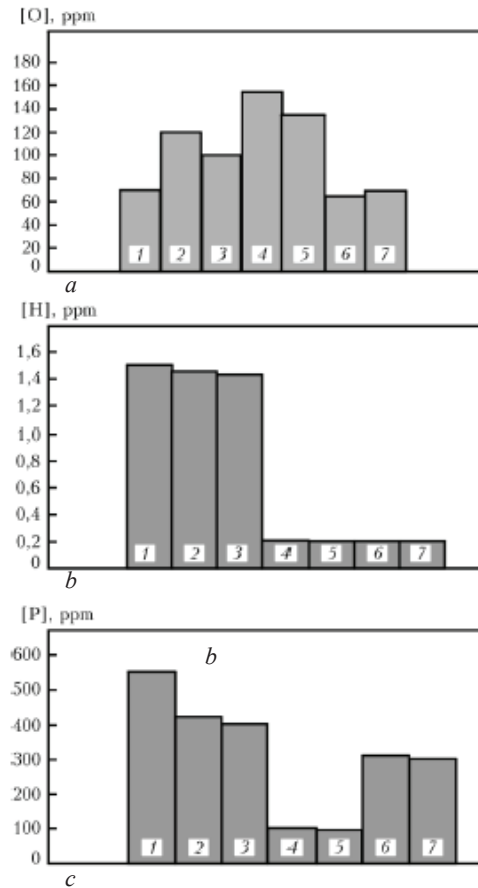
content increased to 0.03% which is almost 50% lower in comparison with the initial charge. The low degree of oxidation of liquid metal during casting is out in an increase of the mass fraction of oxygen in the casting up to 50 ppm which was similar to the content in the initial charge.

Analysis of the results shows that in melting copper by standard technology the presence of oxygen and hydrogen in the casting slightly decreased in comparison with the charge material, but the phosphorus concentration increased.

The melting of copper with oxidation of liquid metal with copper oxide followed by deoxidation resulted in a decrease of the phosphorus content of the castings and a large decrease of the mass fraction of hydrogen in

the castings. The amount of oxygen in the castings remained on the level of the charge materials.

The castings were used for the preparation of flat specimens for experiments with welding of copper to copper and copper to steel. The results show that the welded joints in the metal, produced by oxidation–reduction melting, are characterised by a considerably lower susceptibility to the formation of pores and cracks as a result of the lower hydrogen and phosphorus content.

In subsequent stages, investigations were carried out into the effect of the amount of introduced copper oxide and phosphorus copper and also the holding time between oxidation of liquid metal and its deoxidation on the content of oxygen, hydrogen and phosphorus in the copper castings.

The mass fraction of the copper oxide added to liquid metal was varied in the range 0.5–1.0, the content of phosphorus copper was varied in the range 0.1–0.5%, and the holding time of the melt between oxidation deoxidation was varied between 10 and 30 min.

The results were used to determine the optimum technological parameters and develop a method of refining liquid copper, melting of blanks produced from copper and its alloys in an induction furnace with a graphite crucible.

To reduce the oxygen and hydrogen content of the metal after the oxidation of the copper components of the charge, up to 1.0% of copper oxide was added to the melt, depending on the gas content of the initial metal, the melt was hold for 20–25 min, the slag pool was produced from molten borax and then the melt was deoxidised with the calculated (depending on the concentration of the added copper oxide) amount of phosphorus copper and, if necessary, copper was alloyed with components to produce a specific alloy.

To test the method in the plant conditions, melting was carried out in IAT-04S2 open induction furnace with a graphite crucible for 700 kg of molten metal. The copper and bronze BrAZh9-4 were melted. The charge materials were in the form of cathode copper

and copper savings produced in machining of the components of the casting nozzles. To melt bronze, aluminium pigs and iron in the form of bars were added to the melt.

The copper charge weighing 600 kg was melted in the crucible and heated to 1150–1200°C. The copper oxide was added to the melt and the melt was held for a specific period of time with formation of the slag pool from borax. Subsequently, the melt was the oxidised by holding under the slag layer (deoxidation with the crucible carbon) and prior to the casting was additionally deoxidised by adding MF10 phosphorus copper, 20–30% less than the required amount of phosphorus for neutralising the oxygen added to the metal. In the melting of bronze the remaining components of the metallic charge were added to copper after deoxidation through the slag layer.

Molten copper was used for casting ends of the nozzles for blast furnace and steel melting production with a wall thickness of 8–50 mm, weight 5–125 kg. A casting was taken from each melt, sectioned and examine for porosity and the content of hydrogen, oxygen and impurities.

The experimental results show that if the optimum technological parameters are adhered to, it is possible to produce high-quality dense castings with the mass fraction of hydrogen from 1 to 1.5 ppm, the oxygen content of 15–20 ppm, and the total content of the impurities it not exceed 500 ppm.

To produce metallic nozzles, copper components after appropriate machining were welded with the rings made of steel St3 (Fig. 3). Examination of the welded joints between copper and steel shows that there were no pores and cracks in the parent metal and welded joints.

Bronze BrAZh9-4 was used for casting bearing sleeves which were also free from pores and cracks. The hydrogen content was less than 1 ppm, oxygen content 8 ppm, impurity content 700 ppm.

On the basis of the experimental results, the investigated method of refining of copper has been recommended for further application
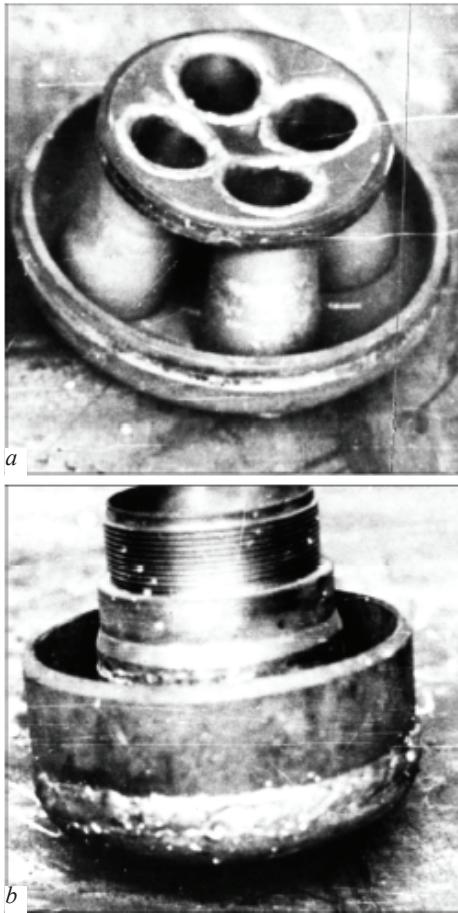
Fig. 3. Metallurgical nozzle: a) cast blanks; b) after machining and welding.

Fig. 4. Content of the following gases in melting of BrKN1-2 bronze from waste: a) oxygen; b) hydrogen; 1) liquid metal; 2) the casting.

in the industrial conditions. The method is relatively simple and cheap but has a number of restrictions: it cannot be used in the melting the waste of copper alloys because in this case the components alloying copper, such as aluminium, silicon,, manganese, zinc, etc, are burnt out.

To get the same time, the large amount of secondary nonferrous starting material consists mostly of the waste of copper alloys (bronze and brass), often fine, low-density, in the form of shavings with higher moisture content and contamination. In most cases, the shavings are processed by remelting in the induction furnaces because the metal after the first melting is often porous and contains a high content of nonmetallic inclusions.

One of the methods of increasing the quality of metal products, produced from the waste of copper alloys, is refining with slags which
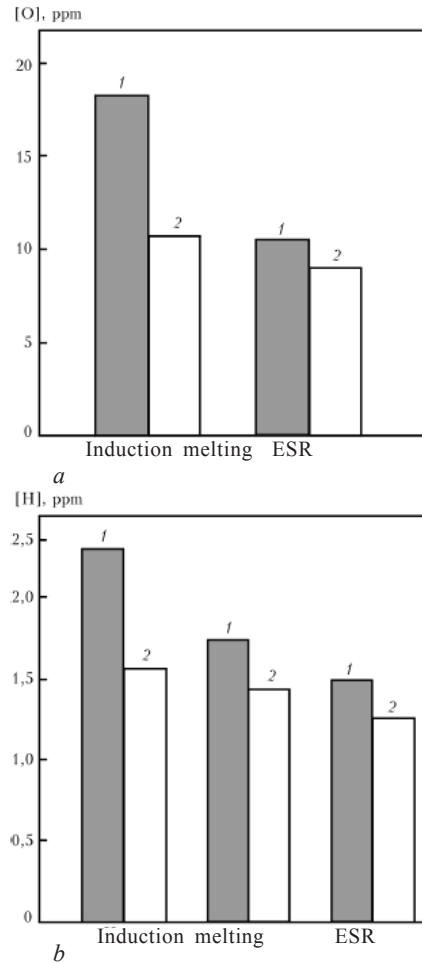
pickup nonmetallic inclusions and dissolve the gas is present in the metal [6, 7].

The refining of the nonferrous alloys with slags can be combined with melting where the slag is used not only as the refining medium but also as the source of heating of metal [8]. This takes place in the electroslag welding with nonconsumable electrodes in which the low-density bulk metallic charge, especially shavings, is gradually supplied into the slag pool, heated as a result of the generation of Joule heat during the passage of electric current through the slag melt.

An advantage of this melting method is that when the metal with higher density falls on the surface of the slag pool this metal melts in the thickness of the slag. The slag melt not only protects the metallic

pool against the surrounding atmosphere but also dissolves hydrogen and oxygen present in the initial metal. In addition to this, in the course of melting it is possible to carry out a deoxidation of the slag and diffusion deoxidation of the metal, and also introduce into the slag components causing the removal of hydrogen from it.

Another advantage of this type of melting is that the metal is subjected simultaneously to cleaning to remove undesirable impurities and the non-metallic components. In this case, the composition of the slag and the temperature conditions of melting can be controlled in wider ranges, and the optimum technological parameters can be selected depending on the composition and the type of processed material.

Figure 2 shows the results of gas analysis of the remelted shavings and waste of KN3-1 bronze in the induction and electroslag furnaces. In both cases, melting was carried out in the graphite crucible. In interaction melting, the surface of the metal was protected with molten borax, and electroslag melting was carried out using ANF-28M slag usually used for melting of copper.

It can be seen that the hydrogen and oxygen content of both the metallic pool and the produced castings in electroslag melting is lower than in the metal produced by double induction remelting. This type of melting also reduces the content of nonmetallic inclusions in the metal which are picked up by the slag. The components made from bronze produced by electroslag remelting were used for the manufacture of various components for important applications which were subjected to tests and the results show that the metal satisfies fully the requirements of technical conditions on this type of material.

Conclusions

1. The experimental results show that oxidation–reduction melting, in comparison with conventional interaction melting, reduces the degree of gas saturation in the phosphorus content of copper.

2. The effect of the amount of the copper oxide and phosphorus copper added to the melt, and also the holding time between oxidation of liquid metal and its deoxidation on the content of oxygen, hydrogen phosphorus in the copper castings was determined.

3. A new method of refining liquid copper and melting of copper blanks and blanks of copper alloys in the induction furnace with the graphite crucible was developed. In the method, after melting the copper components of the charge, to 1% of copper oxide is added to the melt, the melt is held for 20–25 min, the slag pool is produced from molten borax and this is followed by deoxidation of the melt by the calculated amount of the deoxidation agent.

4. The test in the industrial conditions show that if the proposed optimum technological parameters of melting are adhered to, it is possible to produce high-quality dense copper castings with the mass fraction of hydrogen in the range 1–1.5 ppm, oxygen 15–20 ppm (the total content of the impurities did not exceed 500 ppm), and also blanks from BrAZh 9-4 bronze with the hydrogen content less than 1 ppm, oxygen content 8 ppm, and the impurity content of 700 ppm.

5. It has been shown that electroslag melting can be used to produce high-quality metal with the low content of gases and nonmetallic inclusions from fine-dispersion waste of copper-containing alloys.

References

1. Galaktionova N.A., Hydrogen in metals, Metallurgiya, Moscow, 1967.
2. Rabkin D.N., et al., Welding of dissimilar metals, Tekhnika, Kiev, 1980.
3. Paton B.E., (editor), Welding of nonferrous metals and alloys, Mashinostroenie, Moscow, 2006.
4. Ilyushenko V.M. and Bosak L.K., Avt. Svarka, 1984, No. 4, 67-68.
5. Yudkin V.S., Production in casting of alloys of nonferrous metals, volume 1, Metallurgiya, Moscow, 1967.
6. Baranov A.A., et al., Technology of secondary nonferrous metals and alloys, Vyshcha shkola, Kiev, 1988.
7. Kurdyumov A.V., et al., Production of castings of alloys of non-ferrous metals, Metallurgiya, Moscow, 1986.
8. Biktagirov F.K., Sovremennaya Elektrometallurgiya, 2003, No. 1, 5-9.
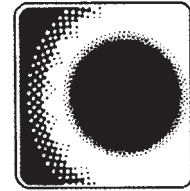
Using the ESA‒ SP method for controlling the chemical composition of fluxes for special electrometallurgy and welding

L.N. Chubov, G.M. Grigorenko and V.V. Lakomskii

E.O. Paton Electric Welding Institute, Kiev

Methodical capabilities of determination of the chemical composition of fluxes for special electrometallurgy and welding using the ESA–ISP method are considered. It is shown that the application of this method allows highly reliable control of not only the element composition of fluxes, but also the content of oxides and fluorides in them that is impossible by other methods.

In the 21st century, the metallic materials have not yet lost their position in engineering and instrument making, aviation, space technology, construction of installations and transport systems.

Engineering, like other branches of industry, requires high quality metal. This problem is solved by special electrometallurgy – the branch formed on the basis of application of welding heating sources for the refining of metal and other operations of metallurgical production.

The processes of welding and special electrometallurgy are being developed continuously, with new concepts and improvement of technology. This also applies to fluxes which are the essential element of the technology of the majority of methods of special electrometallurgy and fusion welding.

On the basis of the chemical composition, the fluxes (slags) are divided into three types: salt, salt–oxide and oxide.

The salt fluxes consists of halides of metals and oxygen-free chemical compounds. The low chemical activity enables these materials to be used in welding and refining in melting of aluminium, titanium and other chemically active metals.

The composition of the salt–oxide slags includes fluorides and oxides. They are used mostly in welding and refining remelting of carbon and low alloy steels.

The high-temperature properties of the slags, especially in the molten condition, are of primary importance for the technological processes of welding and special electoral metallurgy. They include the physical (viscosity, electrical conductivity, surface and

interfacial tension) and physical–chemical properties, which determine the behaviour of the slag in relation to molten metal. These properties of the slags depend greatly on the chemical composition of the slag melt.

The most important function of the slag is the sorption (absorption) of harmful impurities – sulphur, phosphorus and some other elements. The sorption capacity of the slag in relation to the impurities depends on its composition, temperature and the degree of deoxidation of the metal–slag systems. Various conditions are required for the removal of individual impurities. For example, the removal of sulphur is more efficient in the deoxidised system, whereas phosphorus is removed most easily in the oxidation system.

The shielding (covering) properties of the slag are very important for the processes taking place in the arc furnaces and other open systems. The permeability of the slag in relation to nitrogen, hydrogen and oxygen, present in the atmosphere, controls the gas saturation of the metal and the course of oxidation processes. Mass transfer in the slag is associated with the diffusion mobility of the impurities, viscosity and, in particular, the composition of the slag.

The slags may have a number of other functions, depending on the special features of the individual processes – the maintenance of the given thermal conditions, the need to produce the satisfactory surface of the ingot, stabilisation of the electrical arcs, etc.

The most important technological characteristics of the slag is its basicity which is determined in most cases by the ratio of the sums of the concentration of the basic and acid oxides, in the simplest case CaO/SiO_2.

In the sheet, there is a large number of other methods of expressing the basicity suitable for specific conditions. However, it should be remembered that there is no universal scale of basicity and it is necessary to use simpler criteria, if possible.

At the same time, the concept of the basicity has proved to be very useful in practical metallurgy and in welding as the simple generalising characteristic used on a wide scale.

The high-basicity slags are characterised by high sorption capacity in relation to the impurities, fluidity, gas permeability, and support the stabilisation of electric arc. These are 'short for 'slags, i.e., they have a small temperature range of transition from liquid fluid to solid state.

In the same conditions, the acid slags are more viscous, have high insulating properties, a wide range of transition from liquid to solid state ('long' slags).

All these factors indicate that it is very important to control the chemical composition of the flux (slag).
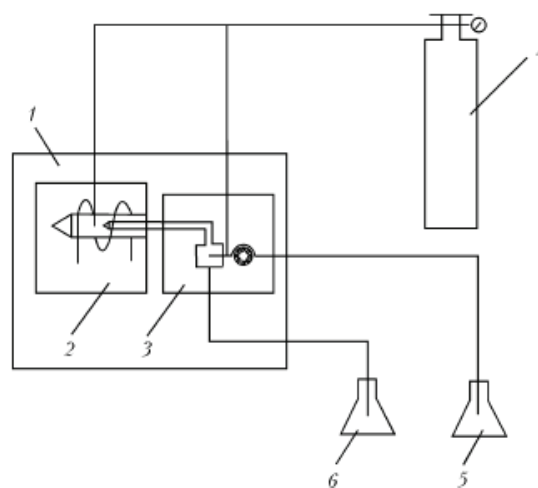
Standard chemical methods [1] have been

Fig. 1. Principal diagrams of ESA–ICP spectrometer: numeral one) electronic–optical unit; 2) the unit with the torch and the induction coil; 3) the sputtering unit with peristaltic pumps; 4) the cylinder with argon; 5) the sample solution; 6) the discharge.
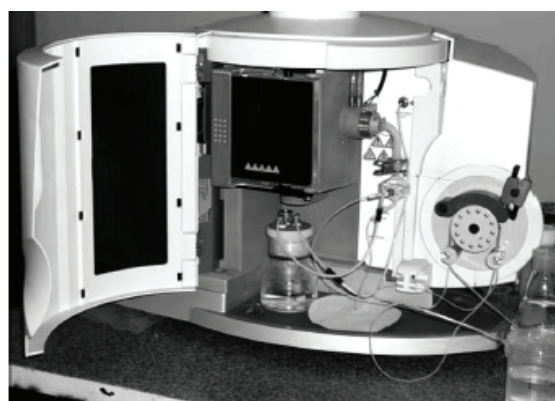

Fig. 2. External view of the ESA–ICP spectrometer.

developed for analysis of the fluxes, and the composition can be determined by x-ray fluorescence analysis [2]. The latter method is fast and not always suitable because of the absence of reference flux specimens.

Insufficient attention has been given to the application of a mission spectroscopy for analysis of the fluxes with excitation by inductively-coupled plasma (ESA-ISP). The setup of the method is shown in Figure 1 and 2.

The traditional advantages of ESA-ISP (the possibility of using for calibration of devices of multi element standard solutions, the wide range of linear calibration graphs, small inter-element effect) enable efficient use of the method in quantitative analysis of specimens with non-standard composition containing, in addition to the mound elements, also impurities of not determined elements [3].

The shortcomings of ESA-ISP include the fact that at the moment it is not possible to determine elements such as oxygen, nitrogen and a number of halides. The obvious advantage of the method applied to special electrometallurgy and welding is the rate of quantitative analysis, no longer than 1–2 hours, were asked complete analysis using the standard methods of separate determination of the elements [1] takes 2–3 days.

The fused welding fluxes consist of oxides of constant composition and fluorspar CaF_2 whose content reaches 30%, and in the fluorite concentrate 80 wt.%. Since initially we determine the concentration of the absolute majority of the elements, including the impunity elements, and this is followed by the determination of their oxides, it may be possible to determine quite accurately the mass fraction of CaF_2 by calculation carried out on the basis of the residual difference.

The promising nature of the investigated method of analytical inspection of the fluxes is confirmed by the fact that, firstly, the direct quantitative determination of fluorine is associated with the application of long-term analysis in energy-consuming equipment which at $CaF_2 > 60$ wt.% gives too low results, of approximately 4 wt.%. Secondly,

the determined error of the procedure of determination of CaF_2 is ±1.5 wt.% which should be regarded as fully satisfactory for the variation, in the majority of fluxes, of the CaF_2 content in the range ±(1…3) wt.%.

The method was developed using the standard fluxes AN-20P, OSTs-45, ANF-60, with the content of the components of these fluxes covering quite extensively the range of components in materials of the same type.

The analytical part of the study consisted of preparation of samples and measurements. A charge of the sample weighing up to 0.2 g was dissolved in the mixture of acids HNO_3 and HF at a ratio of 10:1. The interaction took place in glass–carbon vessels with the addition of 10 ml of distilled water at constant boiling. The resultant solution was transferred quantitatively into a measuring flask and water was added to the mark.

In the presence of an undissolved suspension, the solution was divided into 2–3 parts, and 30 ml of $HClO_4$ and 50 ml of water was added to each part and the solution was again boiled to complete dissolution. When the solutions became transparent, the amount was mixed in the measuring flask to 500 ml. 2–3 aliquotes with 25 ml each were taken immediately for spectral analysis from the resultant solutions. They were diluted using the measuring flask with the volume to ensure that the concentration of the determined elements was within the limits of the linear section of the calibration diagram.

The quantitative dissolution of the alumosilicate materials requires the use of hydrofluoric acid or of its salt. In taking samples, it was necessary to solve the problem of minimising the error in analysis of silicon formed by the dissolution of the glass parts of the dispersion system of the ESA-ISP spectrometer in the medium of F^--ions. To remove the negative effect of their remainder, the required amount of H_3BO_3 was added into the solutions of the samples prior to spectral analysis. The boron ions bonded fluorinr in slightly dissociating compound BF_3.

In the determination of the optimum range of the measured concentration, the dependence
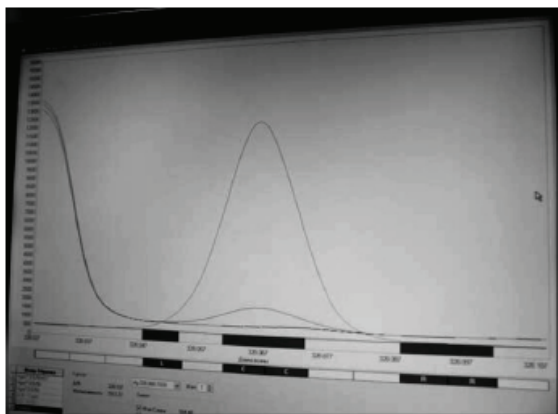
Fig. 3. The image on the screen of the monitor for of the calibrating curve and the readings of the device after processing the analysis results.

of the linear section of the calibration diagrams on the variation of pH of the solutions was determined. To maintain the acidity of the analysed solutions on the level of pH of the standard specimens and reduce the excess concentration of F--ions, and also of boron, the initial solutions were diluted and, if necessary, 1–2 millilitre of HNO_3 was added.

The spectrometry of the elements, included in the composition of the fluxes in the amount greater than 1% and related to the normalised

parameters, was carried out on the basis of 3–5 lines (Fig. 3). The content of the elements – impurities was determined on the basis of 1–2 lines. The lines from which the mutual effect was removed to the maximum extent where considered.

The results of statistical evaluation of the content of the elements in the two samples of the specimen of the flux on three parallel diluted probes show that the relative mean square deviation of the concentration of Sr (%) depends on the absolute value of this concentration and can change in the following ranges: Ca 0.15…0.30; Si 0.15…0.30; Al 0.25…0.45; Mg 0.3…0.6; Mn 0.3…0.5%; Fe 1.5–3.0.

Comparison of the results with the data obtained in x-ray fluorescence analysis of the fluorite concentrate [2] shows that the data obtained by ESA-ISP are characterised by the scatter of the data of parallel measurements 2–5 times smaller. Consequently, the accuracy of calculations determination of CaF_2 is close to that of the direct determination by the x-ray fluorescence method.

These deviations taking into account both possible regularly higher and reduced deter-

Table 1. Comparative evaluation of the content of components in standardized specimens, %

Type of component	Mass fraction of components in standard specimens, %					
	OSTs-45		AN-2011		ANF-6	
	Normative	Determined and calculated	Normative	Determined and calculated	Normative	Determined and calculated
SiO_2	41.7	41.1	23.0	24.0	2.06	2.21
Al_2O_3	2.14	2.33	29.9	30.2	24.6	23.5
CaO acc. to total Ca content	9.86	10.02	23.9	23.1	52.9	52.6
MnO	42.73	42.5	0.43	0.45	—	—
MgO	0.82	0.84	11.4	11.1	—	1.22
Fe_2O_3	0.83	0.78	0.84	0.80	0.13	0.19
$K_2O + Na_2O$	—	0.40	2.36	2.30	—	0.44
Sulphur	0.009	0.01	0.030	0.027	0.020	0.015
Phosphorus	0.085	0.09	0.012	0.014	0.013	0.016
CaF_2	7.02	6.92	28.1	28.3	68.7	69.97
CaO from raw materials	4.80	5.05	3.75	2.73	3.60	2.37
BaO	—	0.80	—	—	—	—
SrO	—	—	—	0.08	—	0.15

mination of silicon (no more than 10 wt.% in calculation to SiO_2) made it possible in the calculations of CaF_2 to reduce the absolute error to 1.5 wt.% (Table 1).

The results also show that when the fluorite content is reduced, the difference systematically decreases. Analysis of the samples showed the presence of compounds of barium and strontium not included in the description of the reference specimens and this confirms the promising nature of using this method for the analysis of fluxes and related materials produced from the initial material with non-constant composition.

Thus, the experimental results show that it is highly promising to use this method for full-scale analysis of the composition of welding fluxes.

References

1 GOST 22974.0-96; GOST 22974.13-96, Welding fused fluxes. Methods of analysis, National Standards of Ukraine, Kiev, 1996.
2 Mikhailova L.V and Kryuchkina T.K., Zavod. Lab., 1999, 65, No. 11, 64-65.
3 Zil'bernshtein Kh.I., High-frequency inductively-coupled plasma discharge in emission spectral analysis, Nauka, Leningrad, 1987.

NEW MATERIALS

Structure and some properties of sodium chloride condensates produced by electron beam evaporation with vacuum deposition

I.S. Kovinskii, L.A. Krushinskaya and B.A. Movchan

E.O. Paton Electric Welding Institute, Kiev

Peculiar features of the formation of sodium chloride by the EB PVD method depending on the condensation temperature are studied. Data of element composition, structural and thermogravimetric analysis are presented.

Introduction

Electron beam evaporation with subsequent condensation of the vapour phase on the substrate (EB PVD) of substances (metals and oxides), together with some halides as the second phase, removed during condensation, was already used previously for the production of a porous structure of thick films and coatings. Examples of the porous structure and possible mechanisms of the formation of the structure were described in [1–3].

Recently, as a result of the development of nanotechnology, special attention has been paid to the development of new materials with different nanoparticles associated with the occurrence of various bioprocesses. Fundamental investigations are now being carried out in the area of nanobiology and nanomedicine.

Some chlorides of alkali metals (NaCl, KCl, $CaCl_2$, $MgCl_2$) are promising as matrixes for various medical substances as a result of their biological compatibility with the living organisms and efficient solution in water (Table 1). Several variants of the formation of nanostructured compounds in the matrix of the chlorides which, if necessary, can already be removed after condensation by the solution in water, were investigated in [3–5].

At the same time, we have not found any literature data on the experiments with the formation of chlorides in electron beam evaporation followed by condensation of the vapour phase on the substrate (EB PVD).

In addition, taking into account the fact that many binary compounds (halides, hydrides, oxides) solidified in the structural type NaCl with the general formula A (including Me) X or MeO, the interest in the processes of formation of sodium chloride from the vapour phase is also scientific in addition to practical [6, 7].

Compound	x	T_{melt}, ºC	T_{evap}, ºC	Density, g/cm³	Solubility, g/100 ml of water at 20ºC	Toxicity
KCl	—	771	1407	1.99	34.4	LD₅₀ 2600 mg/kg [9]
NaCl	—	801	1465	2.16	35.9	Not toxic
$MgCl_2(H_2O)_x$	1, 2, 4, 6, 8, 12	714	1412	2.31	54.8	-
$CaCl_2(H_2O)_x$	1, 2, 4, 6	772	1935	2.15	74.5	-

Comment. Here x is the number of water molecules which can bond the chloride (substance) in crystal hydrate formation.

The production of the condensates and investigation methods

The sodium chloride condensates NaCl were produced by EB PVD using the procedure described in Ref. 3. The general diagram of the process is shown in Fig. 1.
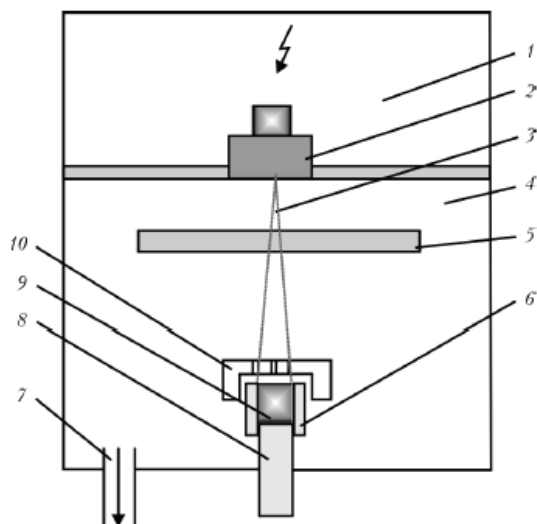
The initial materials were in the form of

Fig. 1. Diagram of the process of electron beam evaporation of chlorides of alkali metals followed by deposition of the vapour flow on the substrate in a vacuum chamber: 1) the gun chamber; 2) the electron beam gun; 3) the electron beam; 4) the working chamber; 5) the substrate; 6) the watercooled crucible; 7) to the vacuum pumps; 8) the bar for supplying the rod; 9) NaCl bar; 10) the graphite cover with the orifices.

Therefore, the aim of the present work was the production, by the EB PVD method, of thick (50–150 µm) sodium chloride condensates and also investigation of their structure and properties.

bars of NaCl (chemical purity grade) produced by cold pressing. Evaporation was carried out from a copper watercooled crucible with a diameter of 50 mm.

To ensure the uniform course of the evaporation process and subsequent condensation, the rate of supply of the bars was maintained constant. Using the cover of the crucible, a system of orifices in which the penetration of the electron beam on the surface of the evaporated material was not allowed was used to ensure the uniform supply of the vapour flow to the substrate. The cover was heated with the electron beam to a temperature of 1200°C (inspected using a W–Re thermocouple).

The vapour flow was condensed on substrates of two types: made of St3 steel with the temperature gradient of 100–600°C, and a watercooled copper substrate with a temperature of 35–55°C. The substrate temperature was controlled using chromel–alumel thermocouples.

The mean thickness of the condensates was 50–150 µm, deposition rate 5–15 µm/min.

Further investigations were carried out on the brittle condensates separated from the substrate.

The microstructure was examined on the surface and cross sections (in the direction of condensation) using scanning electron microscope CamScan 4D.

Statistical analysis and processing of the images of the microstructure were conducted using a specialised set of programs for computer analysis of images Media Cybernetics

image analysis program, Image-Pro Plus version 6.0.

The elemental composition of the condensates was determined by x-ray spectrum microanalysis (EDX attachment to the microscope CamScan 4D). The results were processed using the program INCA-200 Energy, the error of measurements was ±0.3%.

The phase composition and dimensions of the structural components were estimated using x-ray diffraction analysis (DRON-4-07, in CuK_α radiation).

The thermal stability of the condensates was investigated by thermal gravimetry (TGA7, Perkin Elmer, USA, sensitivity up to 0.1 µg) in the atmosphere, in the temperature range 20–650°C. The heating/cooling rate was 10°C/min.

Experimental results and discussion

The produced condensates NaCr were white matt in colour in the entire condensation temperature range investigated.

Since in the operation of money compounds with different volatility the chemical composition of the vapour and the condensates does not always coincide with the initial composition, special attention in the investigations was paid the determination of the elemental composition of the condensates.

In the present case, the components sodium and chlorine are characterised by a large difference in the physical characteristics which could influence the process of evaporation and condensation (Table 2). Nevertheless, the determination of the elemental composition showed that the methods used can be used to produce from the vapour phase condensates with the uniform distribution of elements in the thickness (the scatter of the values was ±0.5%). In addition, the stoichiometric

Table 2. Some physical characteristics of sodium and chlorine

Substance	T_{melt}	T_{evap}	Vapour tension at 100°C, mPa
	°C		
Na	97	883	14.32
Cl	–101	–39	3.81

composition of the investigated chlorides in the entire investigated substrate temperature range according to the results of a large number of measurements did not change, the ratio of sodium and chlorine (at.%) was approximately 0.98±0.02.

Thus, in the temperature range 50–500°C the sodium chloride condenses almost without any change of the chemical composition and retains its stoichiometric composition.

The experimental results show that the formation of the structure in EB PVD is controlled by the deposition temperature T_d.

The structure of the natural surface of the NaCl condensates and the microstructure of the cross sections in the direction of condensation at different substrate temperatures is shown in Fig. 2.

The experimental results also show that, according to the morphological features, these condensates differ for different T_d. The condensates produced in the conditions of low-temperature condensation ($T_d \leq 70$°C) have the structure close to globular and above this temperature they have a columnar structure.

The size distribution of the crystals at different substrate temperatures is shown in the form of histograms in Fig.3.

With increase of the deposition temperature from 80 to 230°C, the size of the crystals rapidly increases (from 0.8 to 4.0 µm). A further increase of temperature in condensation to 400°C has almost no effect on the size of the crystals.

The investigated condensates contain pores, i.e., cavities between the crystals. The shape and dimensions of pores are related with the structure of the crystals. The width of the sections of intercrystalline porosity in the zone of the columnar crystals increases with increasing T_d to 0.8–1.2 µm. At the conversation temperature higher than 400°C porosity decreases as a result of sintering of the crystals.

The variation of the mean crystal size and of porosity of the NaCl condensates in relation to substrate temperature is shown in Fig. 4.

Thus, the experimental investigations of the structure shows that in EB PVD of NaCl
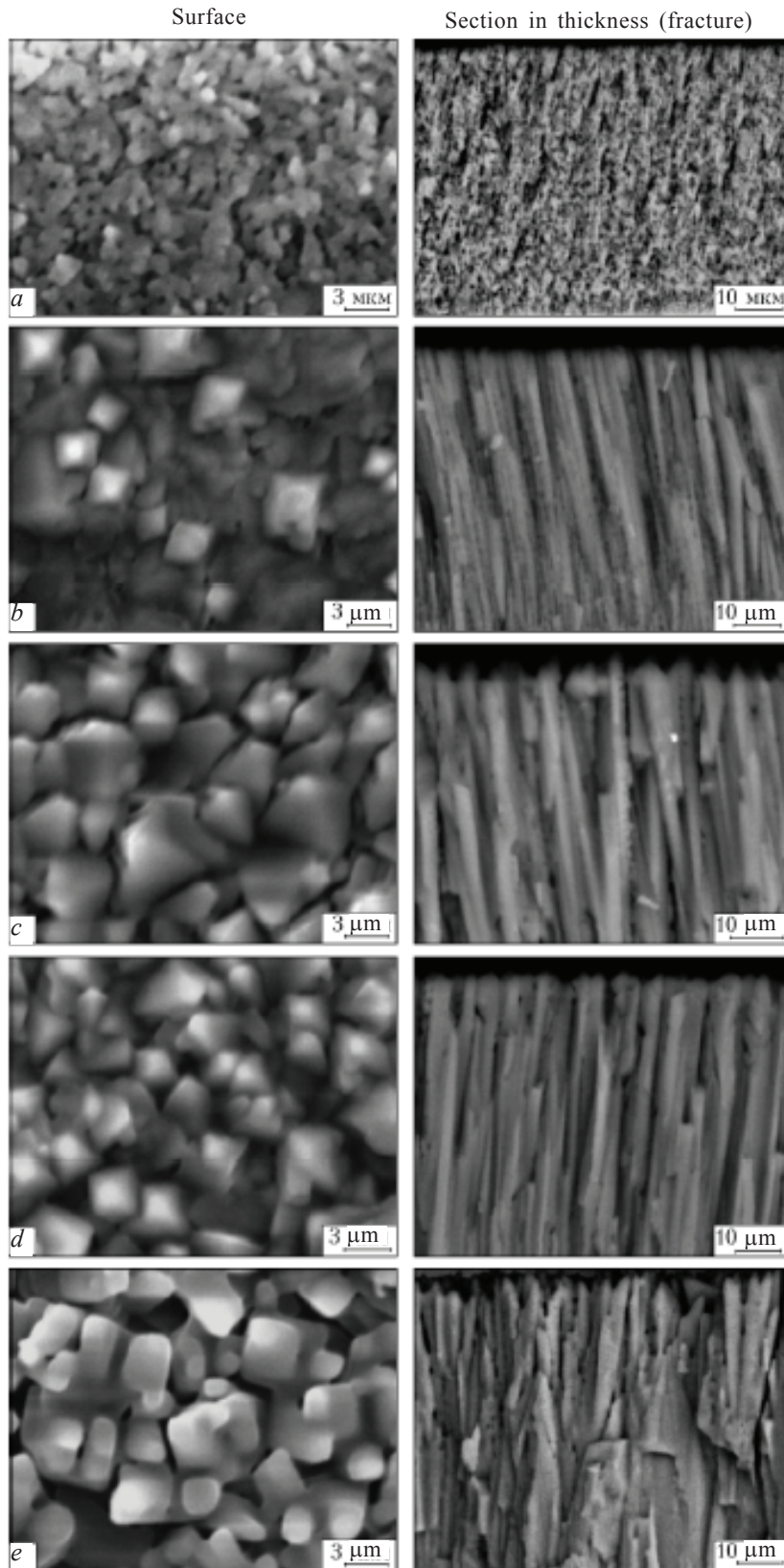
Surface
Section in thickness (fracture)

Fig. 2. The structure of NaCl condensates at different condensation temperatures, °C: a) 50; b) 190; c) 230; d) 400; e) 500.
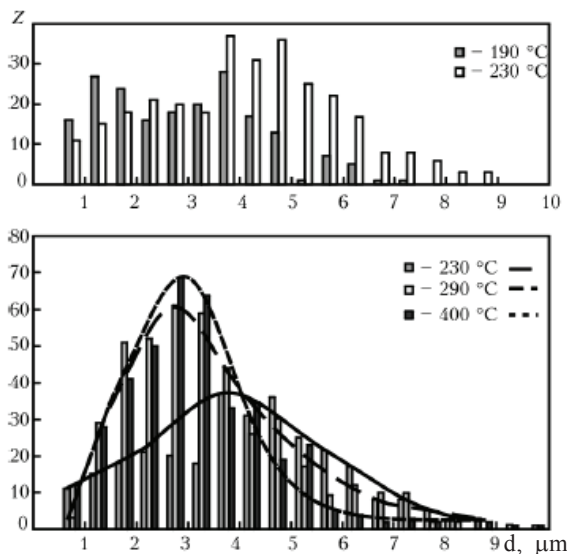
Fig. 3. The size *d* distribution of the crystals in the NaCl condensates at a different condensation temperature, °C; a) 190 and 230; b) 290, 330 and 400; Z is the number of crystals.
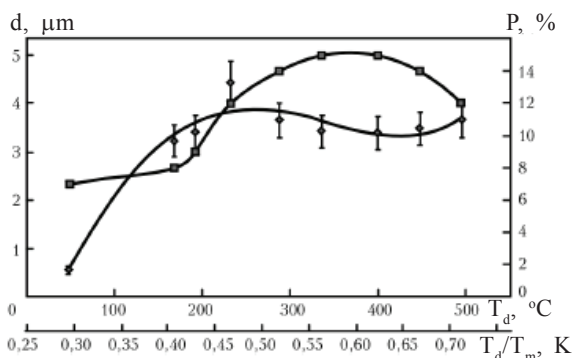

Fig. 4. The dependence of the mean size of the crystals *d* and porosity *P* of the NaCl condensates on the condensation temperature.

there are relationships characteristics of the condensates of other inorganic substances. Depending on the condensation temperature, three structural zones with the boundary temperatures of T_1 and T_2 were found. This is in complete agreement with the diagram of the structural zones [8]. The columnar structure for NaCl was found in the condensation temperature range ($T_1 = 0.3\ T_m < T_d < T_2 = 0.55\ T_m$).

X-ray diffraction analysis of the initial NaCl condensates showed that the resultant condensates are single-phase in the entire temperature range T_d. The parameters of the elementary cell of NaCl at different condensa-
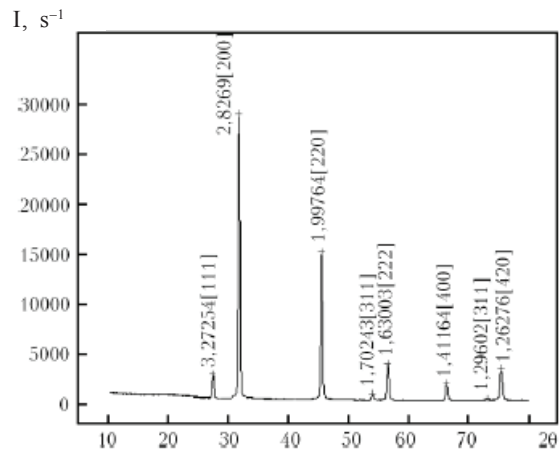

Fig. 5. Diffraction diagram of NaCl: Td = 50°C; T is the intensity of the lines of the measured substance.

tion temperatures deviates slightly (reduction by 0.09%) from the reference value ($a_r = 0.5640$ nm).

Figure 5 shows the diffraction diagram of NaCl which was condensed on the watercooled substrate at a temperature of approximately 50°C. The maximum size of the crystals (calculated using the Scherrer equation) for these NaCl condensates was 57 nm. Thus, these conditions result in the formation of a condensate with the nanocrystalline structure.

The thermal stability determines the service life of the majority of the nanostructured materials and, therefore, the investigations of the thermal stability of these condesates are of both theoretical and practical interest.

The variation of mass in heating was 0.4% (Fig. 6). This mass loss is associated evidently with the removal of adsorbed moisture. In preheating of the NaCl condensates there was no variation of the mass.

During heating, the parameters of the elementary cell of NaCl at each fixed temperature were measured. According to the results of x-ray diffraction studies, the x-ray diffraction diagrams of the annealed specimens and of the initial specimens are almost identical. Thus, the lattice parameters of the NaCl condensates in the investigated temperature range (up to 650°C) is not affected by the annealing temperature, $a = (0.5636 \pm 0.0002)$ nm and corresponds to the reference value (Fig. 6).

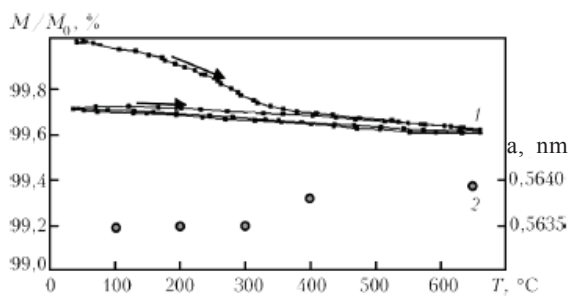In the investigation of the nanoparticles in

Fig. 6. Variation of the mass of the NaCl condensates, T_d = 50°C into heating/cooling cycles (1); the lattice parameter a of the NaCl condensates (T_d = 50°C) at different annealing temperatures.

biology and medicine it is important to pay special attention to the problems of safety because of the possible toxicity of the materials. In the group of the chlorides of alkali metals, characterised by minimum toxicity (Table 1) [9], NaCl is most promising for practical application. However, the range of application of the chlorides of alkali metals, in particular NaCl, is not restricted only to medicine and biology.

For example, in the 1920s, the salt boiling company Diamond Crystal (St Clair, Michigan) published a brochure called 101 methods of using Diamond Crystal salt. In fact, there are many more methods of using sold. The representatives of current salt-boiling industry agree in most cases on 14,000. In the applications that are optics, pharmaceutics, food and light branches of industry, production of fertilisers and agents for melting snow [10–12]. Therefore, the interest in the investigations of the chlorides of alkali metals is still very strong.

Conclusions

1. The electron beam evaporation of NaCl followed by condensation of the vapour phase (EB PVD) is characterised by a number of special features typical of other inorganic materials (formation of three structural zones depending on the condensation temperature).

2. The experimental results show that the zone of the columnar crystals for NaCl forms in the range with the boundary condensation temperatures of $T_1 = 0.3\ T_m < T_d < T_2 = 0.5\ T_m$; the micro- and nanosized porous structure forms at temperatures below T_1.

3. The NaCl condensates, produced by EB PVD, has sufficiently high thermal and chemical stability for practical applications.

4. As a result of the properties of NaCl, such as neutrality in the human organism , high solubility and low hygroscopicity of pure NaCl, this substance can be used as the porous matrix for producing nanoparticles of different substances which will be used in medicine.

References

1. Movchan B.A., et al., Probl. Spets. Elektrometall., 2001, No. 2, 11-14.
2. Movchan B.A. and Yakovchuk K.Yu., ibid, 2001, No. 4, 17-21.
3. Movchan B.A., Zb. Nauk. Prats', 2004, No. 4, 1103-1123, Akademperiodika, Kiev.
4. Movchan B.A., Visnik farmakologii ta farmatsii 2007, No. 12, 5-13.
5. Chekman I.S., et al., Mistetstvo likuvaniya, 2008, No. 5, 32-34.
6. Kasan-Ogly F.A. and Fillipov B.N., Fiz. Met. Metalloved., 2005,15-20.
7. Yalovega G.E., et al., Fiz. Tverd. Tela, 1969, No. 4, 1889-1892.
8. Movchan B.A. and Demchishin A.V., Fiz. Met. Metalloved., 1969, No. 4, 633-660.
9. http//ru.wikipedia.org/khlorid natriya.
10. Kurlanski M., General history of salt, Moscow, 2007.
11. Vladimirov D.A., Optika Spektroskopiya, 2005, No. 1, 147-150.
12. Kukushkin Yu., Chemistry around us, chapter 3, Boiled salt, Vysshaya shkola, Moscow, 1992, 63.

Production of profiled silicon ingots for solar power engineering

Yu.A. Nikitenko

E.O. Paton Electric Welding Institute, Kiev

The main technologies of production of silicon light converters are discussed. Special attention is paid to solar elements manufactured ofrom single crystal silicon. The technological cycle of manufacture of sheets is described. The main manufacture stages in which the production costs increase are. Methods for solving the problem of growing the profiled single crystals are indicated.

As a result of the exhaustion of natural resources, the problem of development of renewable energy sources is very important in power engineering. Scientific teams throughout the world are carrying out investigations to develop equipment for conversion of the energy of natural sources (wind power, wave power, tides, etc) to electric energy.

One of the most promising directions is the application of the solar light radiation, falling on the surface of the Earth, not only for connecting to the world energy system in solving the specific problems of energy saving but also for further exploitation of the solar system and space.

A large number of active elements for converting the solar light to electric energy with a high efficiency coefficient has already been developed. Converters have been constructed on the basis of silicon, gallium arsenide and more complex compounds, including gallium, indium, phosphorus, arsenic, germanium, cadmium, tellurium, and also CIGS systems (copper, indium, gallium, selenium) [1, 2].

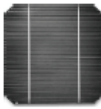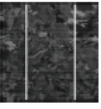The efficiency coefficient of these substances can be greatly increased by the application of nanostructured cascade-type photoelements which represent one of the most complicated semiconductor devices. The presence in the structure of the panel of 20–30 layers ensures the conversion to electricity of not only visible light but also the infrared and ultraviolet sections of the spectrum [3].

However, as a result of the complicated technology of production and the limited reserves of certain chemical elements, the majority of developments remain on the level of laboratory experiments and have no prospects for industrial application. High purity silicon remains the most widely used material for the production of solar panels and semiconductor devices, as previously [4].

Silicon has been used in the development of several types of converters with different structures: amorphous, polycrystalline (multicrystals), single crystal. The converters based on the deposited layers and strips with the amorphous structure are characterised by the lowest efficiency (<10%) and, therefore, the extent of their application is very small.

The main bulk of the light converters is produced from the single and polycrystals silicon. The maximum efficiency of the solar panels based on polycrystalline iron silicon

Table 1. Types of silicon-based converters

Converter type	Form	Dimensions, mm	Efficiency (max),* %
Single crystal		156 × 156	16... 20 (25)
Polycrystal		156 × 156	14... 16 (20)
With amorphous structure		576 × 976	4... 5 (10)

*Maximum efficieny of converters, obtained in laboratory conditions.

remains at approximately 20%, and in the single crystal materials it may reach 25% (Table 1).

The polycrystalline silicon ingots are produced by the melting the purified polycrystalline silicon, the waste and cuttings of semiconductor silicon silicon (Fig. 1, 1). Silicon is melted in the furnaces with a ceramic crucible (quartz, silicon might) and held under specific conditions. In addition, silicon can be subjected to additional processing in vacuum, slags, and gas mixtures, activated in plasma, etc.

Cooling is carried out in accordance with the strictly determined schedule with efficient control of the temperature gradient resulting in the formation of square or rectangular section ingots (Fig. 1, 2). The ingot is then sectioned into parts and subsequently into sheets which are used for the preparation of active elements for solar panels (Fig. 1, 2–6).
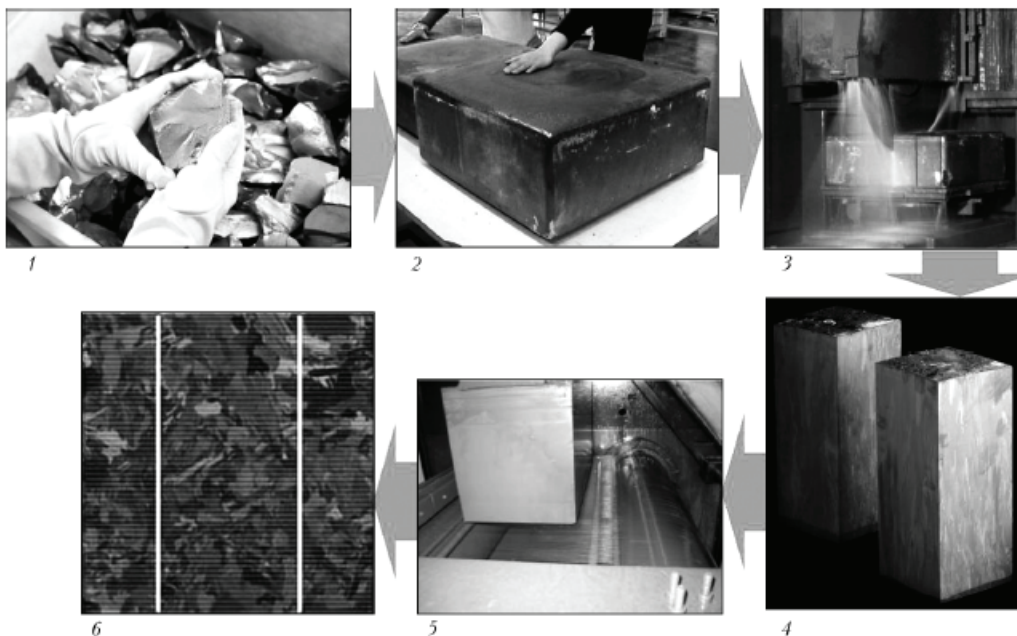
The silicon, produced by this technol-

Fig. 1. Technology of production of ingots of polycrystalline silicon and solar elements from them [5]; for notations 1–6 see the text.
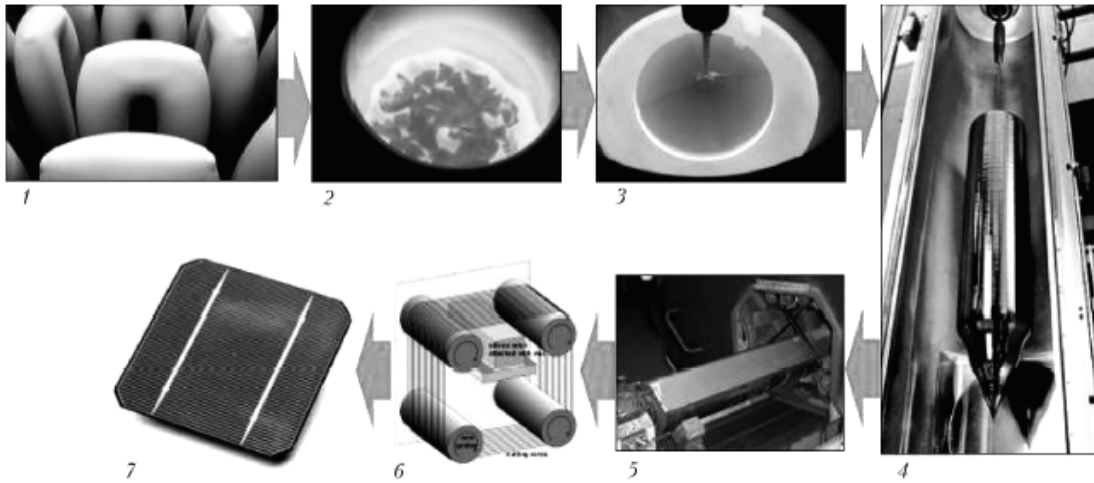
Fig. 2. Technology of production of solar elements from single crystal silicon [7–9]: for notations 1–7 see the text.

ogy is cheaper than single crystal silicon, is characterised by the large crystal structure, but is less efficient in the application as the converter of solar energy.

The reduced values of the characteristics of multi-crystalline silicon are explained in most cases by the higher content of impurities and the presence of the grain boundaries forming additional resistance for movement of charges [6].

The single crystal silicon is grown by two methods: crucibleless zone melting and drawing from the melt.

In crucibleless zone melting the conversion of the polycrystalline bar into the single crystal takes place by the displacement of the molten zone from one end of the bar to the other. The heat source is interaction, electron beam or resistance heating. This technology is designed for a growing silicon single crystals of high purity with a low content of oxygen and carbon.

During growth, the silicon ingots have a relatively small diameter and the increase of the diameter is restricted by the technological special features of the process. At the same time, the price of silicon of this type is relatively high. Therefore, this technology is not used widely in solar power engineering.

The Czochralski method is the basis of the more widely used technology of production of single crystal silicon. The complex process of high purity single crystal silicon consists of the Siemens process and melting of the single crystal by the Czochralski method.

In the first stage, the purified metallurgical silicon is treated with water-free and the reaction results in the formation of the volatile compounds $SiHCl_3$-trichlorosilane (TXC), $SiCl_4$, hydrogen, and also halides of some metals $AlCl_3$, BCl_3, $FeCl_3$, etc. Trichlorosilane is separated from the impurity halides by rectification and a compound with very high purity is produced.

Subsequently, hydrolytic dissociation of TXC in hydrogen takes place in hermetically sealed reactors and this results in the formation of pure silicon which settles on seed bars (Fig. 2, 1). The temperature in the reactor reaches 1100–1150°C, the deposition rate may reach up to 0.5 mm/h. The resultant polycrystalline bars of pure silicon are refined and loaded in a quartz crucible in which the cylindrical ingot of high purity single crystal is grown by the Czochralski method (Fig. 2, 2–4).

The chemical dissociation of trichlorosilane and growth of the single crystal makes it possible to remove almost all harmful impurities resulting in the quality EG-Si (electron grade – 99.9999999%).

Subsequently, the ingot is sectioned (squared) to produce the cross-section in the form of a pseudo-square (Fig. 2, 5).

This is followed by sectioning the ingot into sheets, polishing and production of converters (Fig. 2, 6, 7).

As a result of cutting single crystal ingots and sectioning into sheets, more than 30% of high purity silicon is returned to processing and a large part is lost irreversibly.

Thus, the price of single crystal sheet is considerably higher than that of polycrystalline ones. This is associated with the fact that the entire single crystal silicon is produced in electron grade EG-Si for the production of semiconductor devices in electronics and microprocessor technology.

In solar power engineering, this purity is not required and, therefore, the effective price-quality ratio is ensured by the standard for solar silicon SOG-Si (solar grade, 99.9999%).

The high price of single crystal sheet is also determined by the fact that the method designed for the growth of cylindrical ingot and for the optimum filling of the solar panels are guaranteed by the square shape of active elements (Fig. 3). The currently available technological chain of production of single crystal converters results in their high production costs.

To improve the productivity and reduce the cost of technology, it is recommended to intensify the process of dissociation of trichlorosilane, optimise the refining parameters, i.e., accelerate the process as a result of reducing the quality of silicon. Special attention should also be given to reducing the waste in sectioning and cutting of the ingots, especially in the process of formation of square sections.

The attempts for modernising the technology of growth of single crystals for producing profiles ingots with the given cross-section were carried out many times using methods proposed by Shockley [10] and Stepanov.

The Shockley method is based on correcting the shape of the single crystal by blowing the flow of an inert gas on the solidification front. However, this method is not used widely because of complicated control during the growth process.

Direct blowing of the solidification front results in the oscillations of the melt and this has a negative effect on the formation of the single crystal structure. At the same time, to ensure the high degree of cleaning of silicon, melting and crystal growth should be carried out in vacuum, and the supply of the gas, even after efficient cleaning, has a negative effect on the quality of silicon.

The majority of methods of producing profiled single crystals of semiconductors are based on the method developed by the Russian scientist Stepanov as early as in 1938 [1]. The method is based on placing a floating shaper (die) on the surface of the melt. The solidification front is situated above the surface of the shaper.
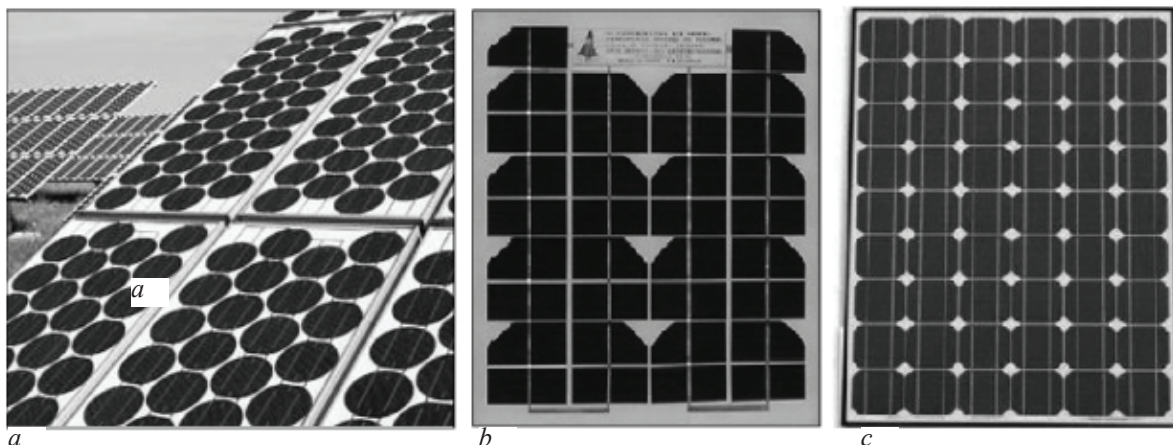
If the required conditions for growth are

Fig. 3. Solar panels, assembled from circular (a), segment (b) and pseudo-square single crystal sheets (c).

fulfilled and the vessel forms of the die are efficiently selected, the method can be used to produce pipes, ribbons and even ingots with a variable cross-section.

The lowering on the solidification front into the depth of the shaper results in the pre-orientation of the crystal or formation of scratches on its surface and other structural defects and shape defects also form.

At the present time, technologies have been developed and single crystal sapphire has been grown together with other components based on Al_2O_3, germanium, lithium nitrate, etc. The Stepanov method gives the results in the growth of compounds of two- and multicomponent crystals for which it is usually possible to select the suitable inert material of the die.

In production of single crystals of high purity elements, the problem of contact of the melt with foreign bodies is quite important. In the majority of cases in growing silicon crystals it is necessary to use a graphite die and, consequently, chemical reactions of these two elements with the formation of silicon carbide take place during crystal growth. In the final analysis, it is not possible to produce a long crystal (Fig. 4) because the crystal loses its single crystal structure (re-orientation, defect formation) take place, the physical properties changes and the crystal is no longer suitable. Therefore, this method is also not used widely for the growth of single crystals of silicon.

It has been attempted to grow singles of various cross-section (square, hexagons) in relation to the orientation of the seed (Fig. 5) [13]. However, this method is not highly efficient. During growth, the crystal and the pool rotate in the opposite directions and, consequently, the phases of the crystal become smooth and the cross-section becomes circular. The side faces of these crystals also become uneven, with a large number of defects, and require further processing.

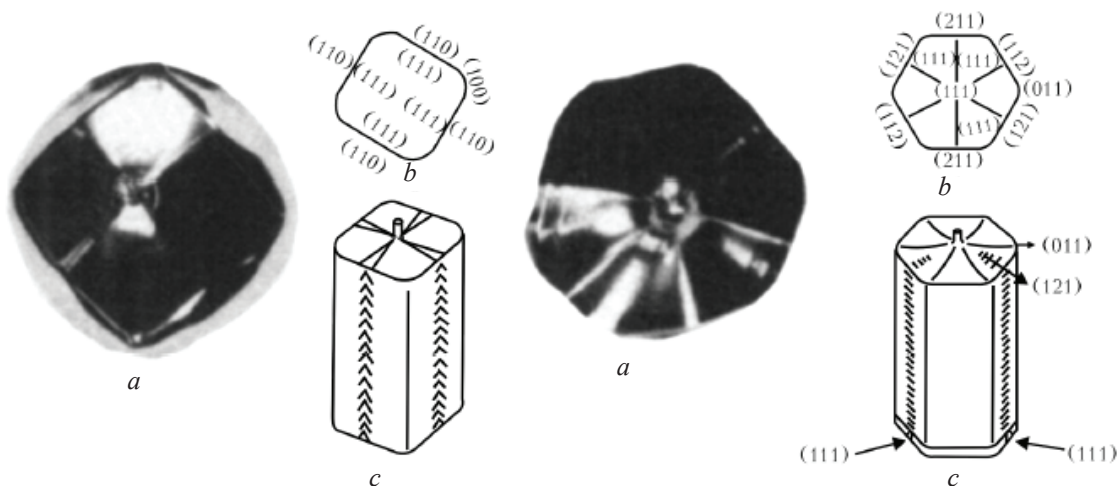**Fig, 4.** Silicon single crystal, grown by the Czochralski method [12].

Fig. 5. The square silicon crystal with the [100] plane (1) and the hexagonal crystal with the [111] plane (2): a) top view of the grown crystal; b) the sketch of the section of the crystal with the projection of the planes; c) the sketch of the crystal.

A positive solution may be the development of a technology and equipment which would make it possible to influence the solidification front and grow shaped crystals with the cross-section close to square. The main principle, used as the basis for new developments, should be directed to producing a temperature field of a specific configuration which influences the shape of the solidification front. This system would make it possible to reduce the losses in the cutting of ingots in the squaring process and this would make it possible to save material and reduce production costs.

The active thermal effect on the solidification front may result in the formation of thermal stresses in the crystal, changes of crystallisation conditions and other negative phenomena. However, the formation of the temperature field does not contaminate of the growing crystals, in contrast to the use of the shaper.

The development of new methods of single crystal growth require additional more extensive investigations. It may be assumed that the develop meant of technology of growing profiled single crystals is essential and would find its application in both solar power engineering and electronics.

References

1. Green M.A., et al., Progress in photovoltaics, Research and Applications, 2006, No. 14, 45–51.
2. Green M.A., et al., IEEE Transactions on Electronic Devices, 1999, No. 46, 1940–1947.
3. Alferov Zh.I., et al., Fiz. Tekh.Poluprov., 2004, No. 8, 937-948.
4. Farenburkh A. and B'yub R., Solar elements: theory and experiments; Energoatomizdat, Moscow, 1987.
5. http://pvdcdrom.pveducation.org,manufact/mc-si.htm
6. Raivey K., Defects and impurities in semiconductor silicon, translated from the English, Mir, 1984.
7. http://www.schott.com/english/news/pres.html?NID=2172.
8. http://ru.wikipedia.org/wiki/method_czochralskogo/
9. http://www.gemtree.com/AWSM/index.htm
10. Maslov V.N., Growth of profiled semiconductor crystals, Metallurgiya, Moscow, 1977.
11. Stepanov A.V., Zh. Tekhn. Fiz., 1959, No. 3, 381-393.
12. http://periodictable.com/items/014.23/index.html.
13. Handbook of semiconductor silicon technology, New Jersey, Park Ridge, 1990.

INFORMATION
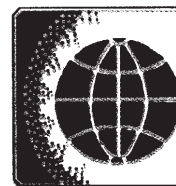
Refining and alloying of titanium in the process of electroslag remelting in a chamber furnace

A.D. Ryabtsev and A.A. Troyanskii

Donetsk National Technical University

The theoretical basis of electroslag remelting of metals and alloys under active slag systems in chamber-type furnaces in a controllable atmosphere (ChESR) is described.

Titanium and its alloys occupy a special position in the group of the promising structural materials adopted in recent years by the industry. The continuous expansion of the sphere of application of these materials in different branches of technology is explained by the favourable combination of their physical and mechanical properties.

Traditionally, titanium alloys are melted using vacuum- and plasma-arc remelting and in recent years also electron beam in melting. The possibilities of remelting processes can be expanded greatly by electroslag remelting of the metals and alloys and active slag systems in the chamber-type furnaces in the controlled atmosphere (CESR).

Experts at The Donetsk National Technical University developed theoretical fundamentals of this process, investigated its main relationships, developed and applied technologies for producing ingots from different metals and alloys, including titanium. The CESR method has all advantages of classic electroslag remelting – the refining slag medium, directional crystallisation and the satisfactory surface quality of the ingot.

The furnace chamber enables remelting of high-reactivity metals and alloys, including titanium alloys, in the controlled atmosphere, and the metallic calcium in the slag systems results in low partial pressure of oxygen and nitrogen in the slag and the gas phase. This creates suitable conditions for refining and alloying.

To apply the process in practice, the results of the investigations were used for designing new equipment, without any large capital investment, to modify the currently available electroslag remelting systems into chamber electroslag furnaces, with the construction of a number of industrial furnaces U-578, USh-148, USh-137 (Fig. 1).
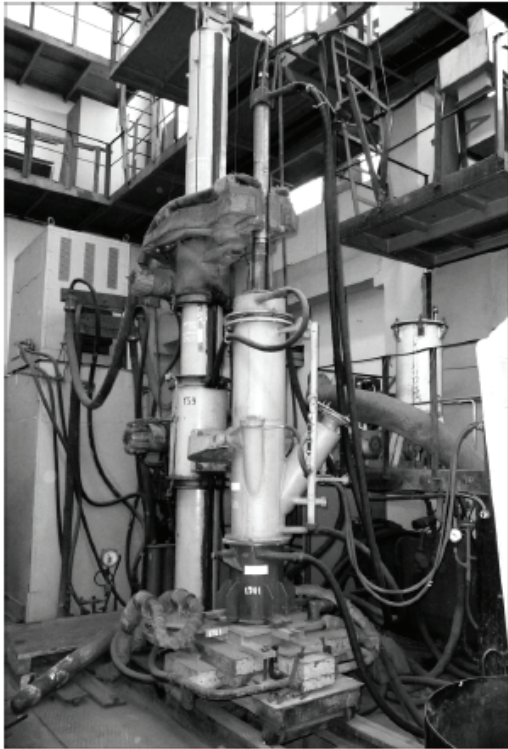
Fig. 1. The chamber electroslag furnace designed on the basis of the U-578 equipment.

The experimental results were used for developing the technology of refining titanium and its alloys to remove oxygen and nitride inclusions, to produce cast ingots with the impurity content on the following level, wt.%: 0.03-0.06 oxygen, 0.005-0.006 nitrogen, 0.003-0.005 hydrogen, 0.01 carbon. The experimental results show that the addition of metallic calcium to the CESR slag results in refining of titanium to remove nitrogen and
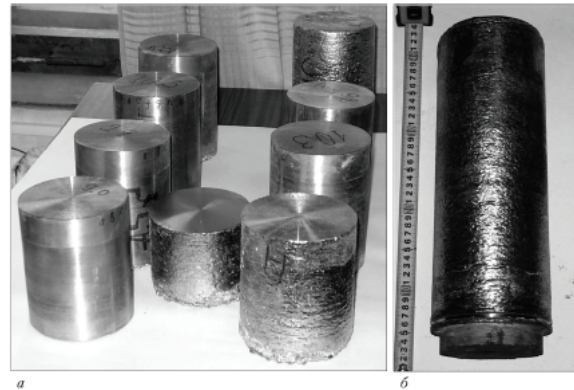

Fig. 2. Titanium ingots produced by CESR.

oxygen by respectively 10–15 and 20–25%.

A technology was proposed for the guaranteed introduction of oxygen from the gas phase on the master alloy into the titanium during remelting of the sponge accompanied by the increase of the oxygen content in the metal by a factor of 2-7 in comparison with the initial content (for the oxygen content of 0.40%).

A technology was developed for producing intermetallics of the titanium-aluminium system, alloyed with chromium, niobium and boron, and also 30–50 at.% of aluminium.

The CESR technology has the following advantages:

– high quality of the ingot (Fig. 2) already after the first remelting (high chemical and structural homogeneity and satisfactory surface which does not require any further

machining);

– guaranteed reduction of the content of harmful impurities;

– the possibility of producing the square and rectangular section ingots;

– utilisation of titanium wastes (scrap, the shavings) followed by production of high quality ingots;

– the refining of the primary titanium-aluminium alloy, produced by the alumothermic method;

– reduced consumption of electric energy;

– application of simpler and cheaper equipment.

The technology has been tested successfully in the laboratory-industrial conditions in the production of titanium ingots with a diameter of up to 200 mm and is recommended for industrial application.

New design of vacuum chambers of electron beam melting furnaces

Yu.V. Neporozhnyi, O.E. Sobko-Nesteruk, N.V. Chaika, V.N. Vasyura, N.G. Tretyak, I.E. Gorchinskii and T.I. Dubovaya

Antares Company, Kiev

The new principles of designing of vacuum chambers, realized in the development of electron beam furnace VT02, designed for producing ingots of round and rectangular section of titanium and titanium alloys (cylindrical ingots of 640 and 825 mm diameters, rectangular ingots of 190 × 1325, 250 × 1325, 420 × 1325 mm and length of up to 5.5 m) are described.

The vacuum chambers for melting, withdrawal of the ingot, loading and supply of the charge, included in the composition of the electron beam furnace are the most important and labour-consuming sections both in the period of preparation of design documentation and in the process of manufacture, testing, setting and assembling. The design solutions for each of these vacuum chambers should take into account a number of specific requirements which control the required parameters of the furnace and normal functioning of all sections, mechanisms, the energy system and the control system is in service. It is also important to guarantee the safe conditions of operation of servicing personnel during manufacture, testing, setting, assembling and service.

The following main requirements imposed on the design of the vacuum chambers:

– the dimensions, form, cross-section of the vacuum chamber should be selected on the basis of the conditions of rational distribution of the mechanisms, sections and ease of servicing, loading the required amount of the charge, minimisation of pumped volumes;

– the vacuum chamber should be characterised by the required values of mechanical strength of the walls and given rigidity;

– the design of the vacuum chambers and wall thickness should satisfy the requirements of biological protection of personnel against the effect of x-ray radiation, formed in the deceleration of accelerated electrons in the material of the melted components;

-the vacuum chamber should be safe for the servicing personnel in the case of sudden disconnection of electric power supply or failure of operation of the cooling system and the system for arresting the operation of the electron beam furnace;

– the vacuum chamber should be fitted with high-speed devices for reliable sealing in the areas of vacuum sections (covers, doors);

– the design of the vacuum chamber should include the operating systems for finding leaks for the diagnostic self important vacuum sections (covers, doors, the late of the electron beam guns, vacuum chambers – melting and the ingot).

The design team at the Antares company developed a VT02 electron beam furnace of a new generation with the rated power of the electron beam guns of 3.2 MW, the annual productivity of titanium of up to

Table 1. Technical and economic parameters of vacuum chambers with different wall cross sections

Cross section	Calculated element of the wall of the vacuum chamber	Calculated inertia momentum, cm^2	Maximum calculated deflection, mm	Specific metal capacity, t/m^2
Rectangular		7560	0.84	1.12
Box		17515	0.36	0.85

3000 t. This design took into account the previously mentioned requirements imposed on the vacuum chamber for electron beam furnaces.

The form of the cross-section of the vacuum chambers for the supply of the charge is rectangular with the size of 1000 × 1560 mm so that it includes the melting front is 700 × 1020 mm in size which are approximately 1.5 times greater than the area of the melting front of the previously used furnaces. It should also be mentioned that this form of the cross-section and its dimensions make it possible to compose rationally the charge feed mechanism with the stroke of up to 5700 mm and the capacity of the charge of up to 8 t in every vacuum chamber. The capacity of the charge is up to 1.6 times greater than the parameters of the vacuum chambers for supply of the charge of the existing electron beam furnaces.

All the vacuum chambers of the electron beam phase are characterised by the required mechanical strength of the walls and the minimum losses of metal for production as a result of utilising the experience with the design of vacuum chambers of equipment for electron beam welding where the selection of the calculated parameters of the cross-section of the wall and the box section of the power system is justified. The ratios of the geometrical parameters, economic and mass parameters are presented in Table 1.

The high rigidity of the chamber walls is essential in the cases in which precision mechanisms are mounted on the walls (charge supply, ingot withdrawal). Deformation of the walls of the vacuum chamber under the effect of atmospheric pressure may differ and, consequently, displacement (linear, angular) of the elements of the mechanisms, based on them, should correspond to the requirements on precision of operation. For example, the mechanisms for supplying and withdrawing the ingots for the VT02 electron beam furnace can operate in a stable manner at maximum deformation of up to 0.8 mm along the length of the stroke of the pushing devices for the charge and the trail of the bottom plate, equal to 6550 mm.

The thickness of the walls of the vacuum chamber should correspond to the requirements of biological protection of personnel, according to the standards of radiation safety

(SRS) against the effect of x-ray radiation, formed in deceleration of the accelerated electrons on the heated surface. The total thickness of the walls of the vacuum chambers of the VT02 electron beam furnace was selected at 22–24 mm, which corresponds to the SRS standards for the accelerating voltage in the cathode of the electron beam gun of 50 kV.

When disconnecting the power supply and demand the cooling system in the system for arresting operation of the electron beam furnace fail there is a danger of unsealing of the vacuum volumes (the plate of the gun, the colour of the vacuum chamber for supply of the charge, the vacuum chamber for melting, all possible nozzles of the vacuum system) as a result of thermal failure of the rubber and synthetic seals. This may cause explosion of oil vapour pumps and burning of the titanium charge or titanium alloys.

To prevent these undesirable phenomena, all the walls of the vacuum chambers of the VT2 furnace are characterised by a large distance between the internal and external shelves creating large volumes filled with water. The volume of the vacuum chambers of the VT02 furnace is approximately 14 m; the weight of the chambers approximately 36 t.

The temperature of cooling water in the case of a failure of the cooling system will be estimated. The amount of heat, accumulated by water and the mass of all the chambers $Q_{\Sigma(1+2)}$, can be determined from the following relationship:

$$Q_{\Sigma(1+2)} = M_1 C_1 \tau_{75^\circ C} + M_2 C_2 \tau_{75^\circ C} = 5.65 \cdot 10^9 \text{ J},$$

where M_1 is the mass of water (14 million g); M_2 is the mass of the chambers (36 million g); 75°C is the maximum permissible different temperatures of water from 100°C to the initial temperature at entry into the vacuum chamber of 25°C, which ensures that the seals of the vacuum sections are not affected and are leaktight when the electric power supply is switched off and the cooling system fails; C_1 is the mean heat capacity of water (4.19 J/g); C_2 is the mean heat capacity of steel (0.46 J/g).

The value $Q_{\Sigma(1+2)}$ should be equal or slightly smaller than (but no more than by 10%, taking into account the cooling of the vacuum chambers by the atmosphere of the production shop) and the heat content level Q_3 of the heated ingot weighing 10 t at the moment of this connection of the power supplied with the furnace or failure of the cooling system. The heat content Q_3 of the heated ingot is as follows:

$$Q_3 = M_3 C_3 \tau_{m \cdot ing} = 5.95 \cdot 10^9 \text{ J},$$

where M_3 is the mass of the heated ingot (10 million g); C_3 is the mean heat capacity of titanium and its alloys (0.7 J/g); $\tau_{m.ing}$ is the mean temperature of the ingot at the moment of this connection of the power supply of failure of the cooling system, equal to 850°C and an ingot mass of 10 million g. Taking into account the calculation results and comparison of the values of $Q_{\Sigma(1+2)}$ and Q_3 it may be concluded that the VT02 electron beam furnace is safe in the case of sudden this connection of the electric power supply or when the cooling system fails.

It should also be mentioned that the reliability and safety of service of the VT02 electron beam furnace are showed by the application of high-speed vacuum gates of oil vapour vacuum pumps, with the activation time of 1–2 s.

The vacuum chambers of the VT02 electron beam furnace are fitted with devices for rapid and reliable sealing of all the vacuum sections (the cover, the plate of the guns, doors), associated with loading and servicing of the mechanisms during service. The speed and reliability of ceiling are controlled by the removal of conventional clamping devices (pressure bolts, screws,) which are time-consuming when used. Vacuum tightness of the contacting surfaces is guaranteed. The initial clamping of the doors, covers, the plate of the guns is achieved by the use of clamping rollers, multifunctional guides, ridges and displacement suspensions, ensuring efficient contact of the sealed surfaces. Final securing is realised by the atmospheric pressure during

Fig. 1. Design of the device for moving and sealing the doors of the chamber for supply of the charge.
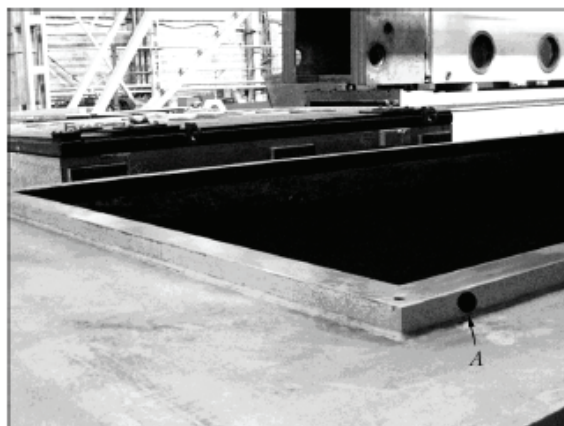

Fig. 2. The design of the flange of the chamber for the supply of charge for inspecting the vacuum tightness of the welded joints: A) the hole in the flange of the vacuum chamber.

pumping. A suitable example is the device of the doors of the vacuum chamber for the supply of the charge (Fig. 1).

To carry out operational diagnostics, the important vacuum sections of the VT02 electron beam furnace are fitted with a system for finding vacuum leaks. The typical example of application of these systems (for the vacuum seal of the loading section in the vacuum chamber for the supply of the charge) is shown in Fig. 2 where all the welded joints are checked for penetration of the atmospheric air around the perimeter through the hole in the flange A of the vacuum chamber.

The new design solutions, satisfying these requirements, have been used in developing and constructing an electron beam furnace which greatly differs from the currently available furnaces by technical and economic parameters.

Thus, the vacuum chambers of the VT02 furnace have the metal requirement 1.5 times lower (weight has been reduced from 90 t to 65 t). The labour content and cost of production have been correspondingly reduced. The reduction of the pumped volume of the vacuum chambers of the furnace from 95 to 62 m^3 reduces the time required to establish the working vacuum by approximately 1.5 times so that the productivity of operation of the furnace can be improved as a whole.

It is also important to mention that regardless of the reduction of the mass and the dimensions, the productivity of the VT02 electron beam furnace increased, in comparison with the VT01, from 2500 to 3000 t/year with respect to titanium. The weight of the melting ingots increased from 10 000 to 14 000 kg, the length of the ingots from 4.0 to 5.5 m.